Electronic Supplementary Material (ESI) for Organic & Biomolecular Chemistry.

Supplementary Material

Stimuli-responsive Transmembrane Anion Transport by AIE-active Fluorescent Probe

Nasim Akhtar, Oindrila Biswas, Debasis Manna[*]

*** Correspondence:**

Debasis Manna

Email: dmanna@iitg.ac.in

Table of Contents:

1. Synthesis and characterization of compounds:

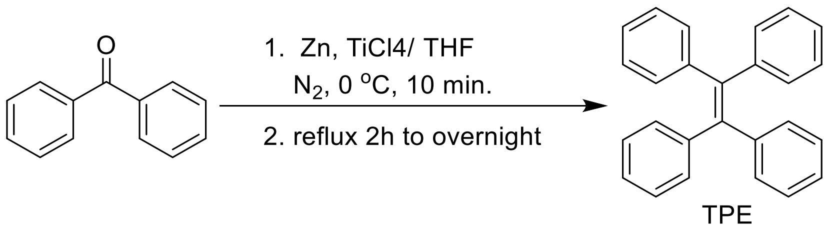

Scheme S1 Synthesis of 1,1,2,2-tetraphenylethene.

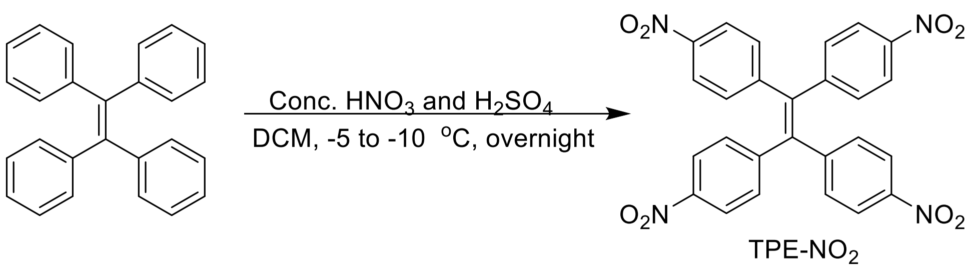

Scheme S2 Synthesis of 1,1,2,2-tetrakis(4-nitrophenyl)ethane.

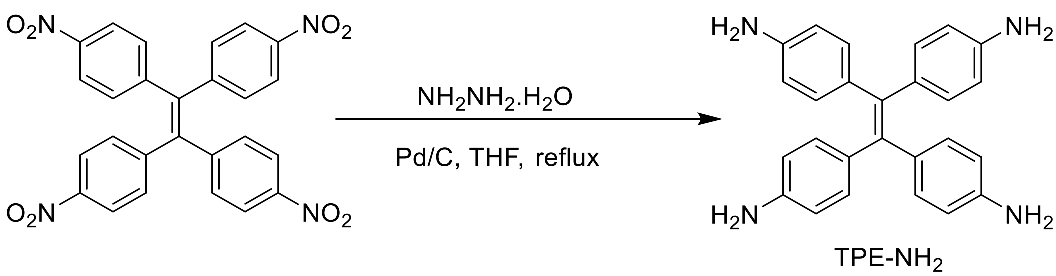

Scheme S3 Synthesis of the 4,4',4'',4'''-(ethene-1,1,2,2-tetrayl)tetraanilin.

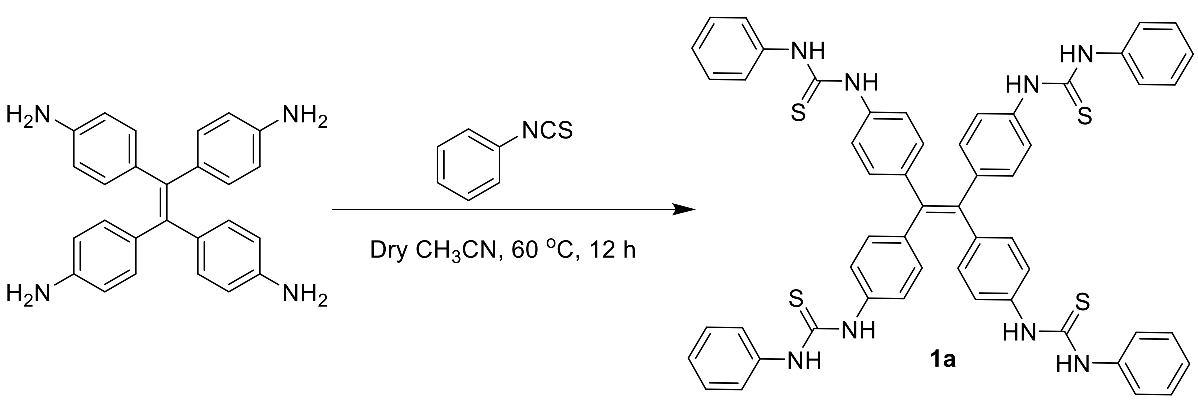

Scheme S4 Synthesis of TPE-based compound **1a**.

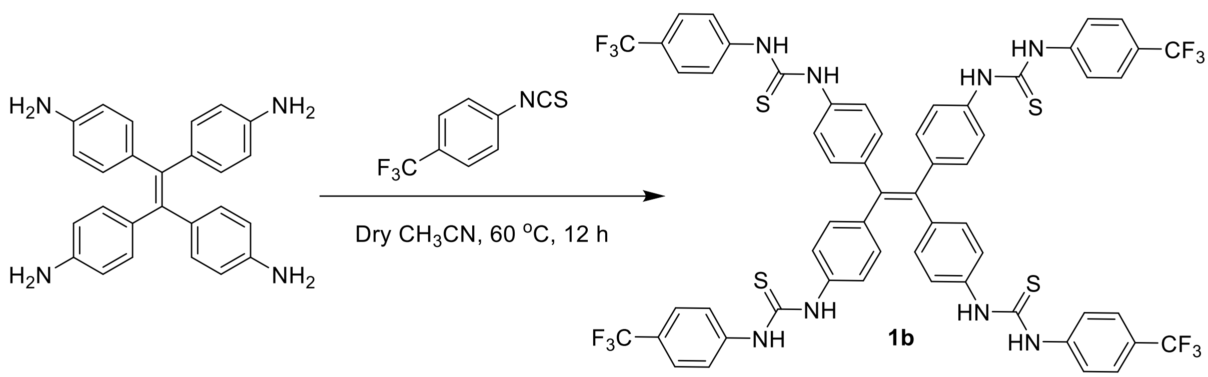

Scheme S5 Synthesis of TPE-based compound **1b**.

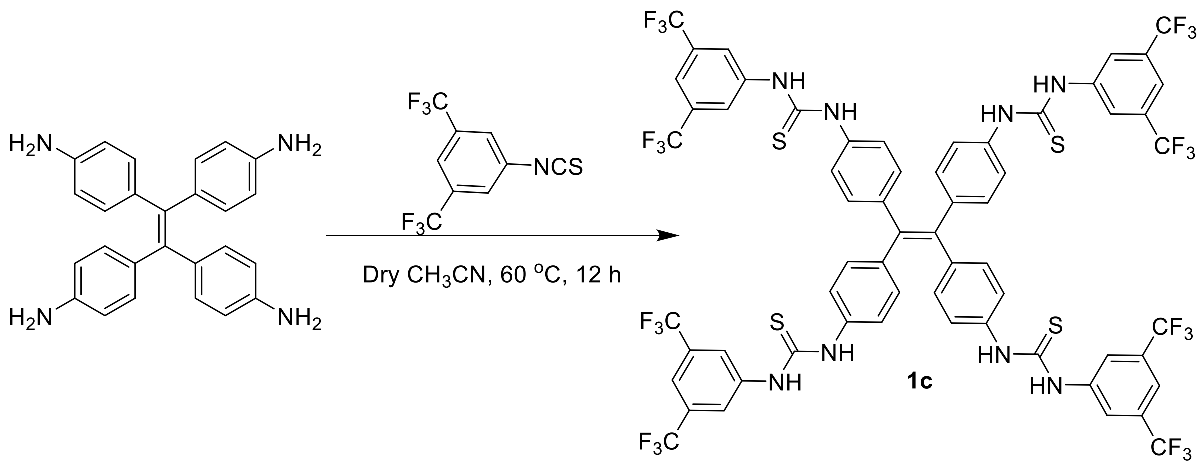

Scheme S6 Synthesis of TPE-based compound **1c.**

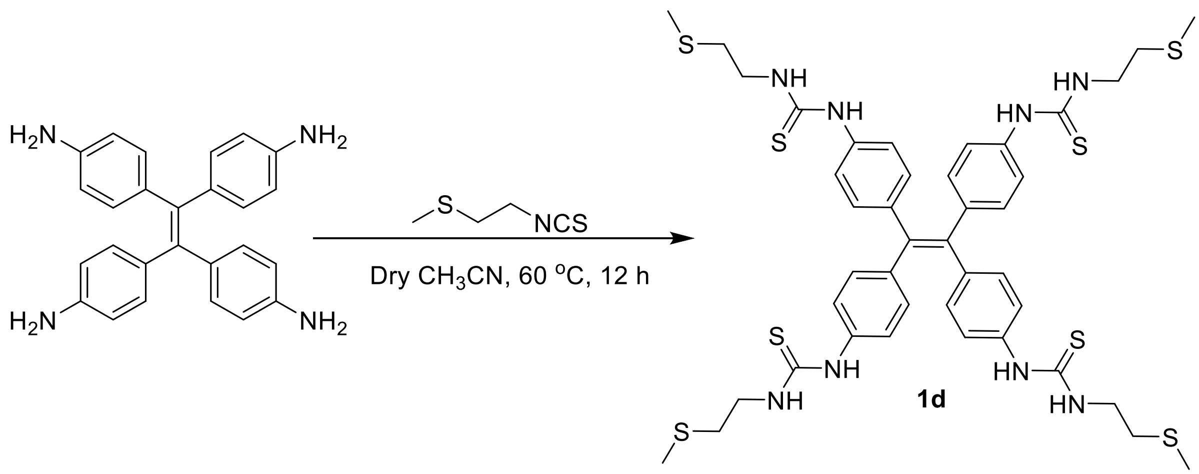

Scheme S7 Synthesis of TPE-based compound **1d.**

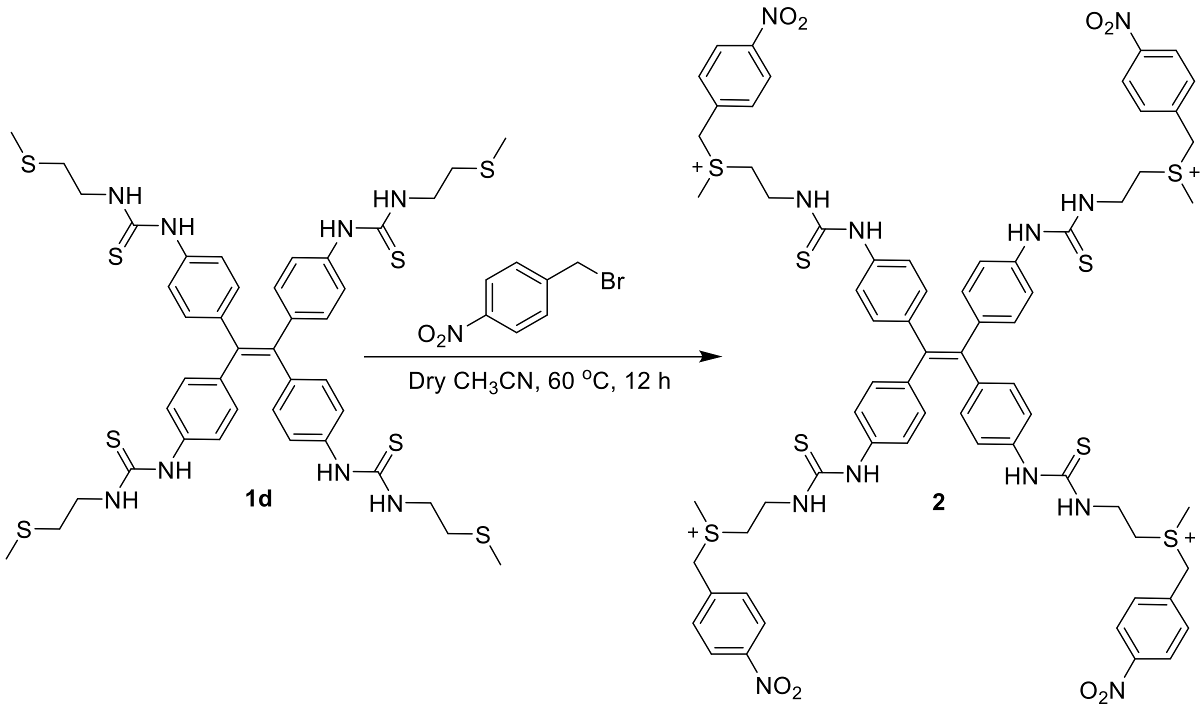

Scheme S8 Synthesis of proanionophore **2.**

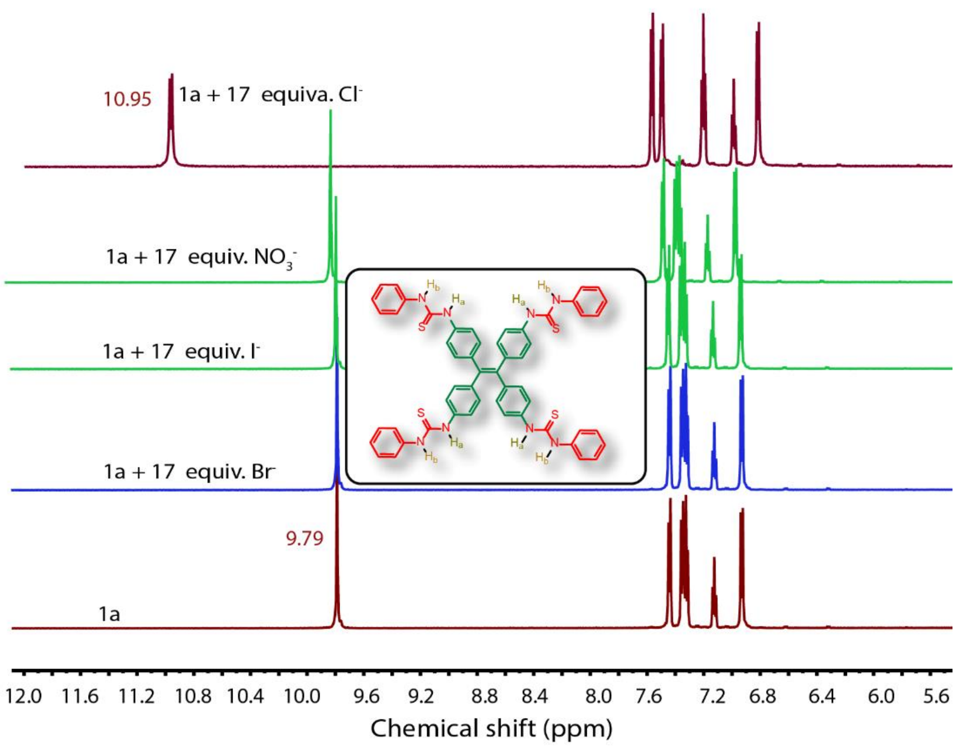

Fig. S1 The ^{1}H NMR titration spectra for compound **1a** (3.45 mM) with a fixed concentration of numerous anions salt of TBA (58.65 mM) in DMSO-d_6 solvent at room temperature.

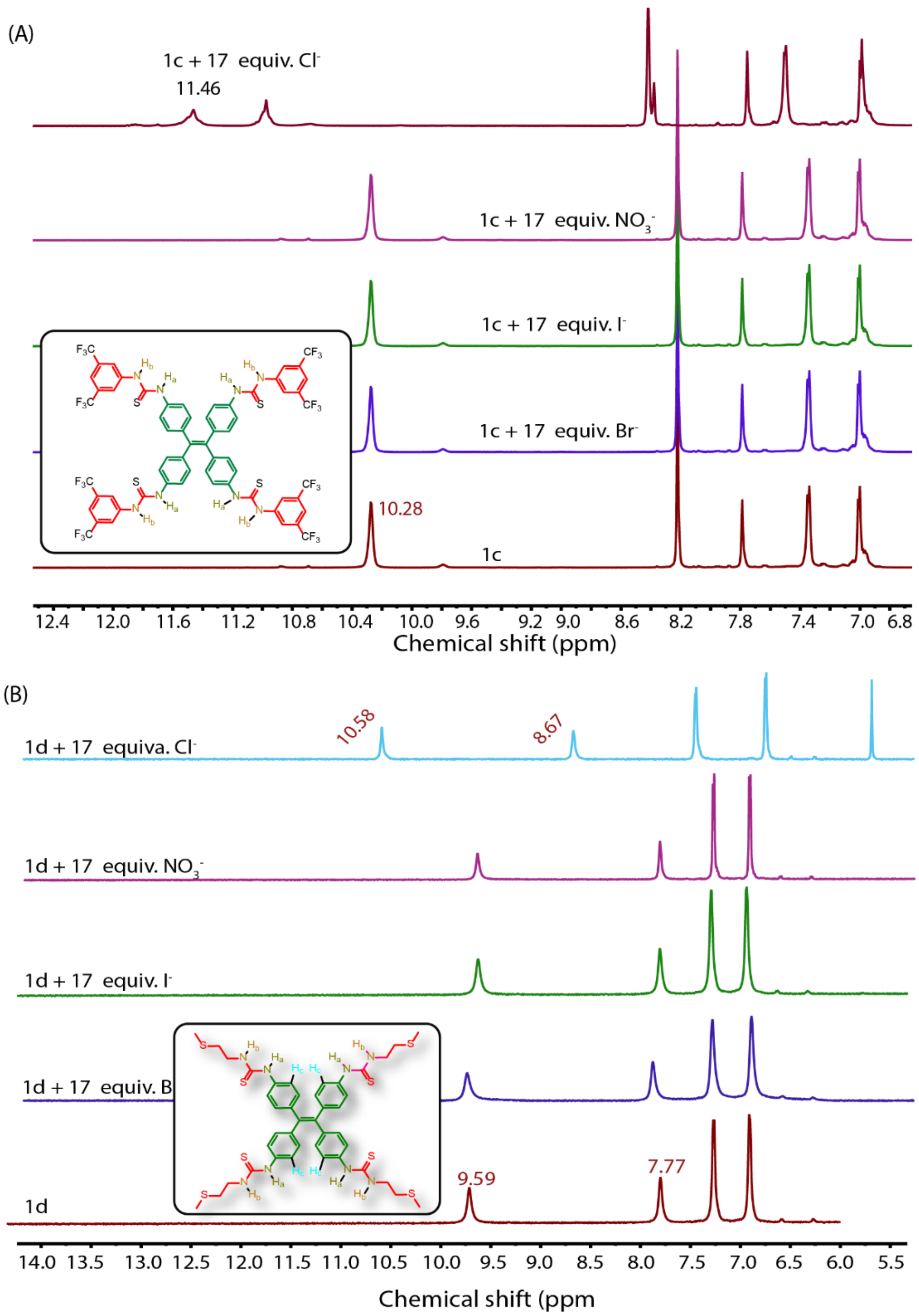

Fig. S2 The ^{1}H NMR titration spectra of compound **1c** (A) and **1d** (B**)** (3.45 mM) with a fixed concentration of various anions of TBA salts (58.65 mM) in DMSO-d_6 solvent at room temperature.

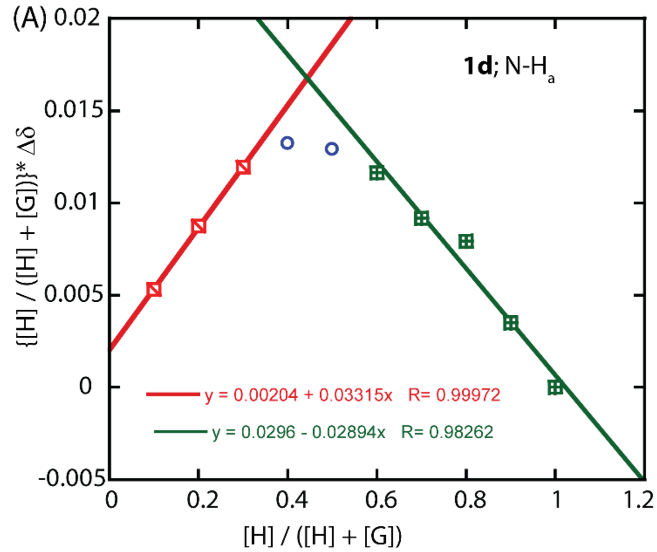

Fig. S3 Job's plot analysis for **1d** with TBACl in DMSO-d6 solvent by varying mole fraction of **1d** against the chemical shift of N-H_a (A) and N-H_b (B).

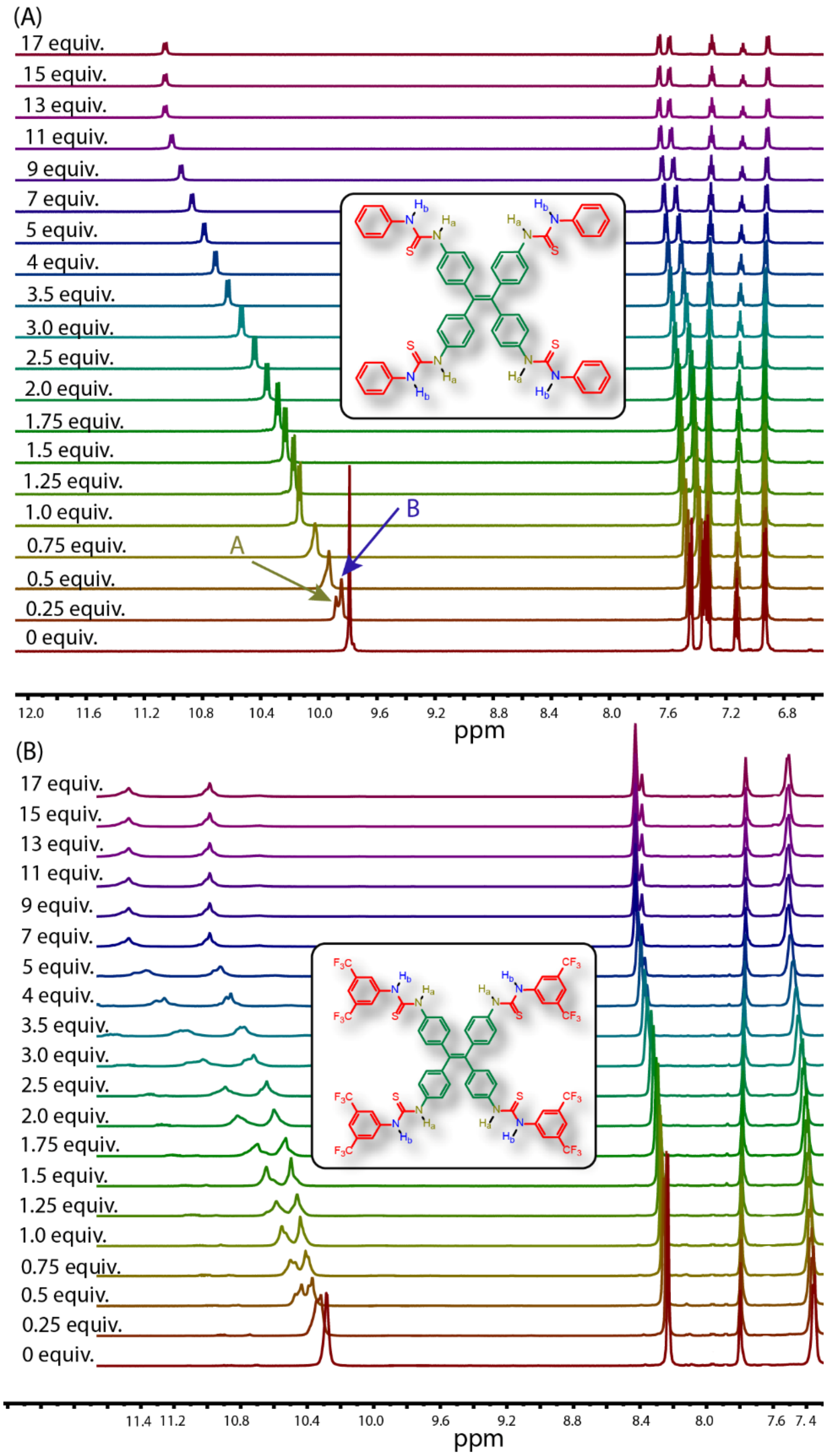

Fig. S4 ^{1}H-NMR (600MHz) titration spectra for compound **1a (A) and 1c (B)** with the chronological addition of TBACl in DMSO-d_6 solvent, respectively. The equivalent amounts of added TBACl were shown on the spectra.

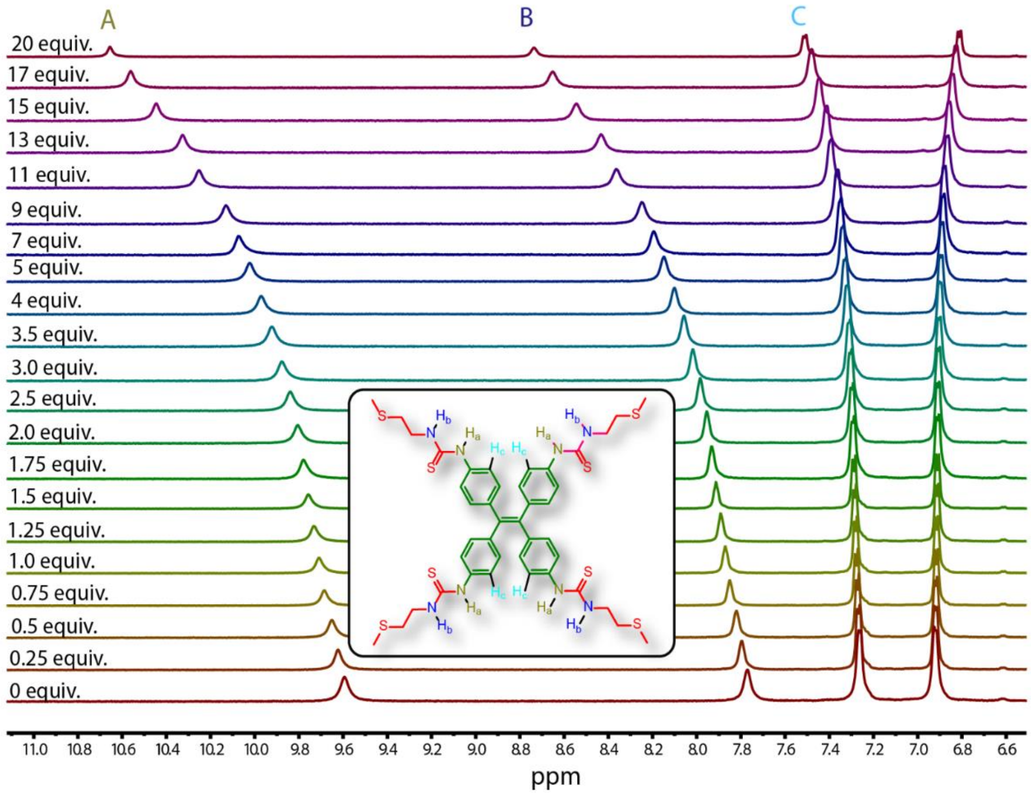

Fig. S5 ^{1}H-NMR (600MHz) titration spectra for compound **1d** with the chronological addition of TBACl in DMSO-d_6 solvent. The amounts of added TBACl were shown on the spectra.

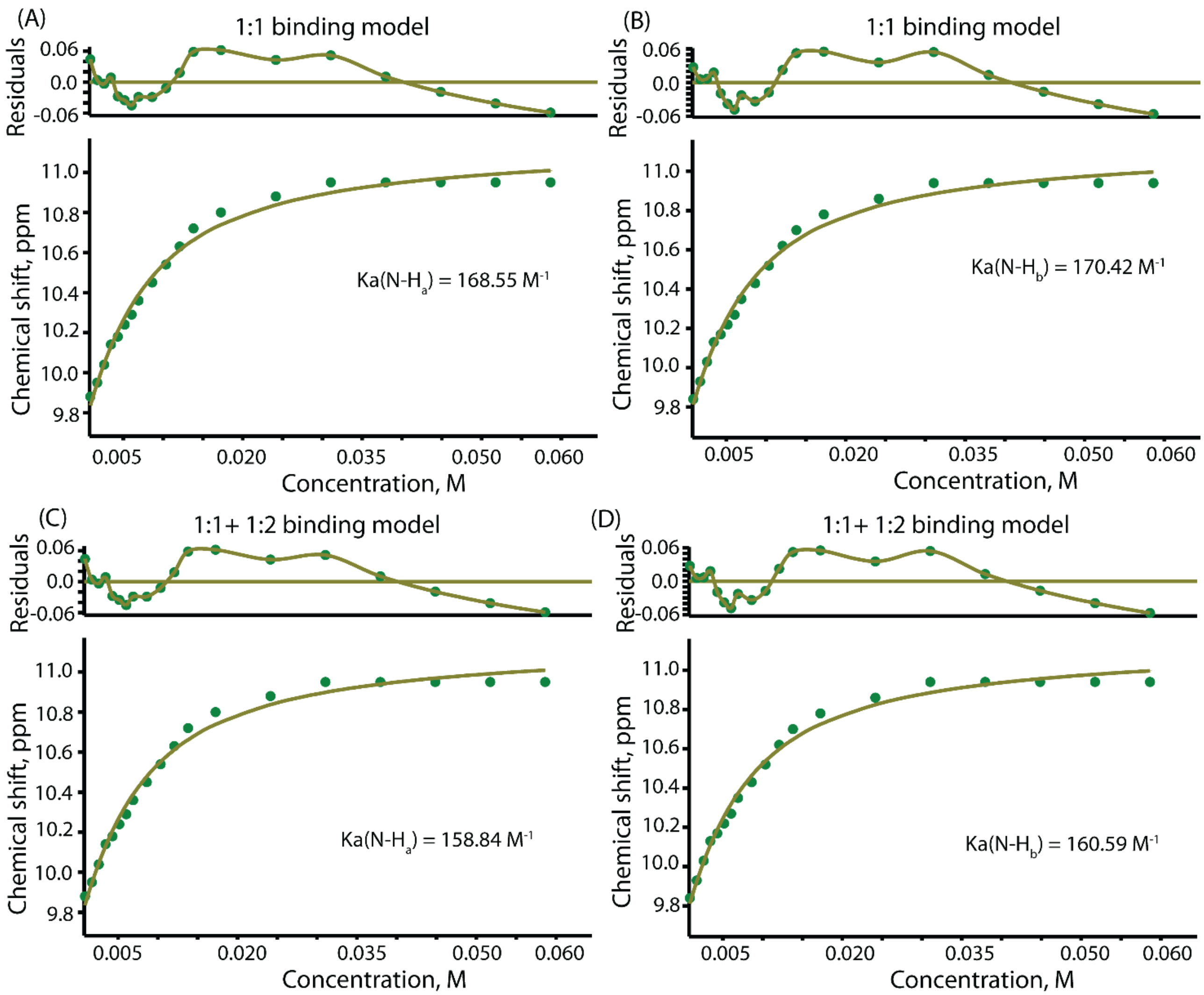

Fig. S6 Plots of non-linear fit using WinEqNMR and experimental points (symbols) against the concentration of TBACl for **1a** in DMSO-d_6 solvent mixture using either N-H_a (A, C), N-H_b (B, D) with 1:1 or a mixture of 1:1 and 1:2 host/guest stoichiometries.

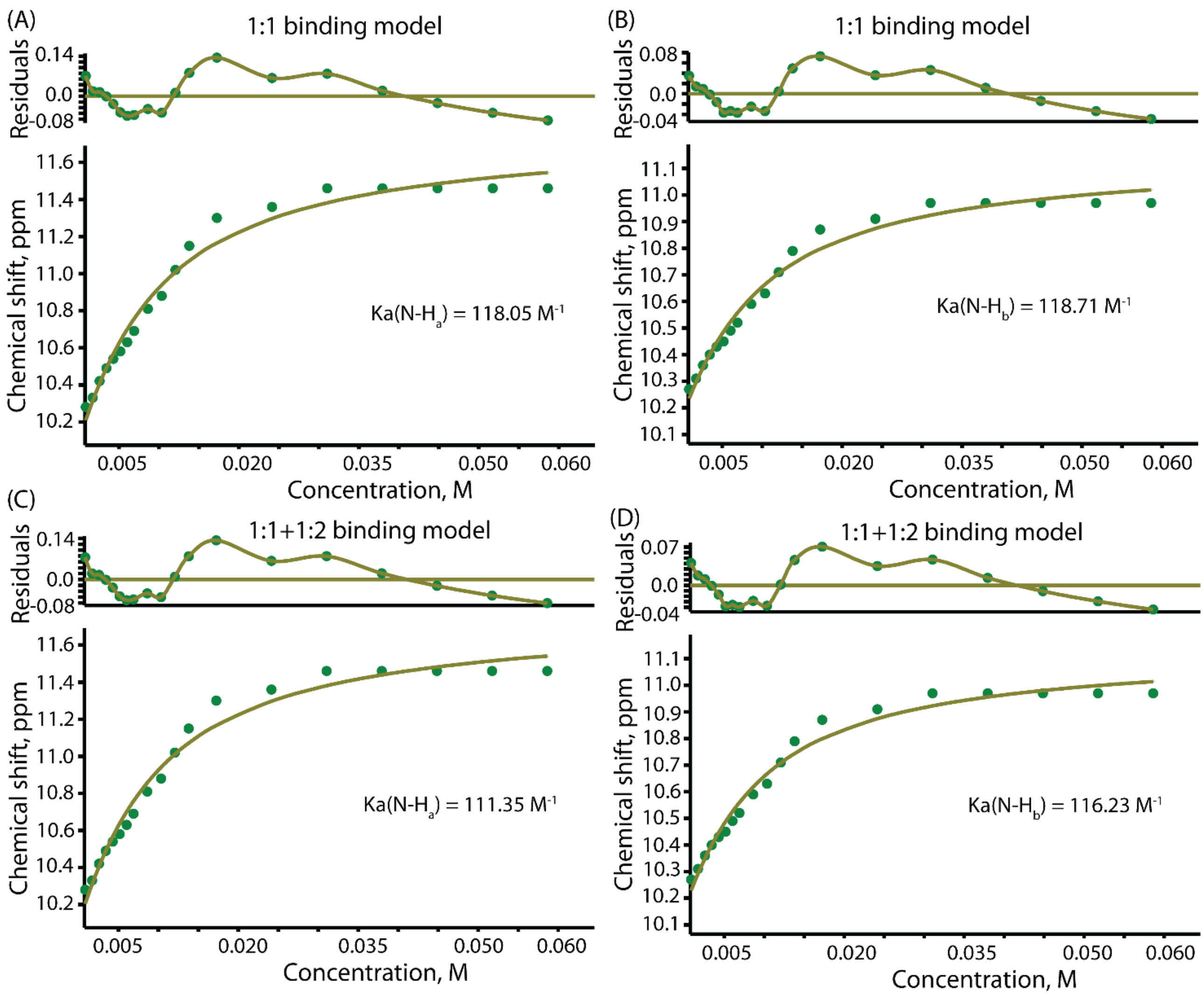

Fig. S7 Plots of non-linear fit using WinEqNMR and experimental points (symbols) against the concentration of TBACl for **1c** in DMSO-d_6 solvent using either N-H$_a$ (A, C), N-H$_b$ (B, D) with 1:1 or a mixture of 1:1 and 1:2 host/guest stoichiometries.

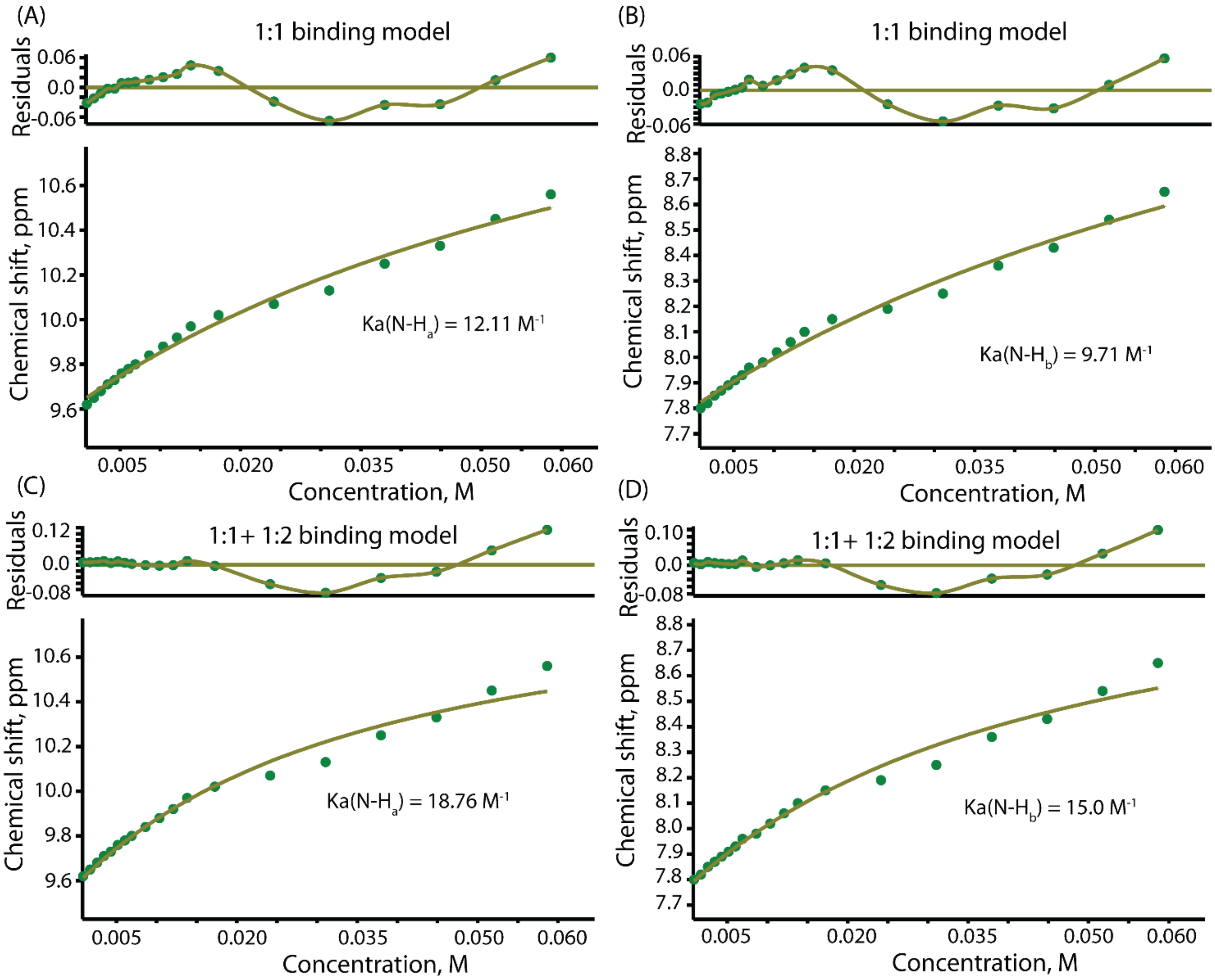

Fig. S8 Plots of non-linear fit using WinEqNMR and experimental points (symbols) against the concentration of TBACl for **1d** in DMSO-d_6 solvent mixture using either N-H_a (A, C), N-H_b (B, D) with 1:1 or a mixture of 1:1 and 1:2 host/guest stoichiometries.

Table S1. Binding affinities of the compounds.

1:1 binding model		
Compound Code	K for N-H_a	K for N-H_b
1a	168.55	170.42
1c	118.05	118.71
1d	12.11	9.71
1:1 + 1:2 binding model		
1a	158.84	160.59
1c	111.35	116.23
1d	18.76	15.0

N.B. Due to the broadening of N-H peaks, binding affinities from the ^{1}H NMR could not be measured for compound **1b** compound.

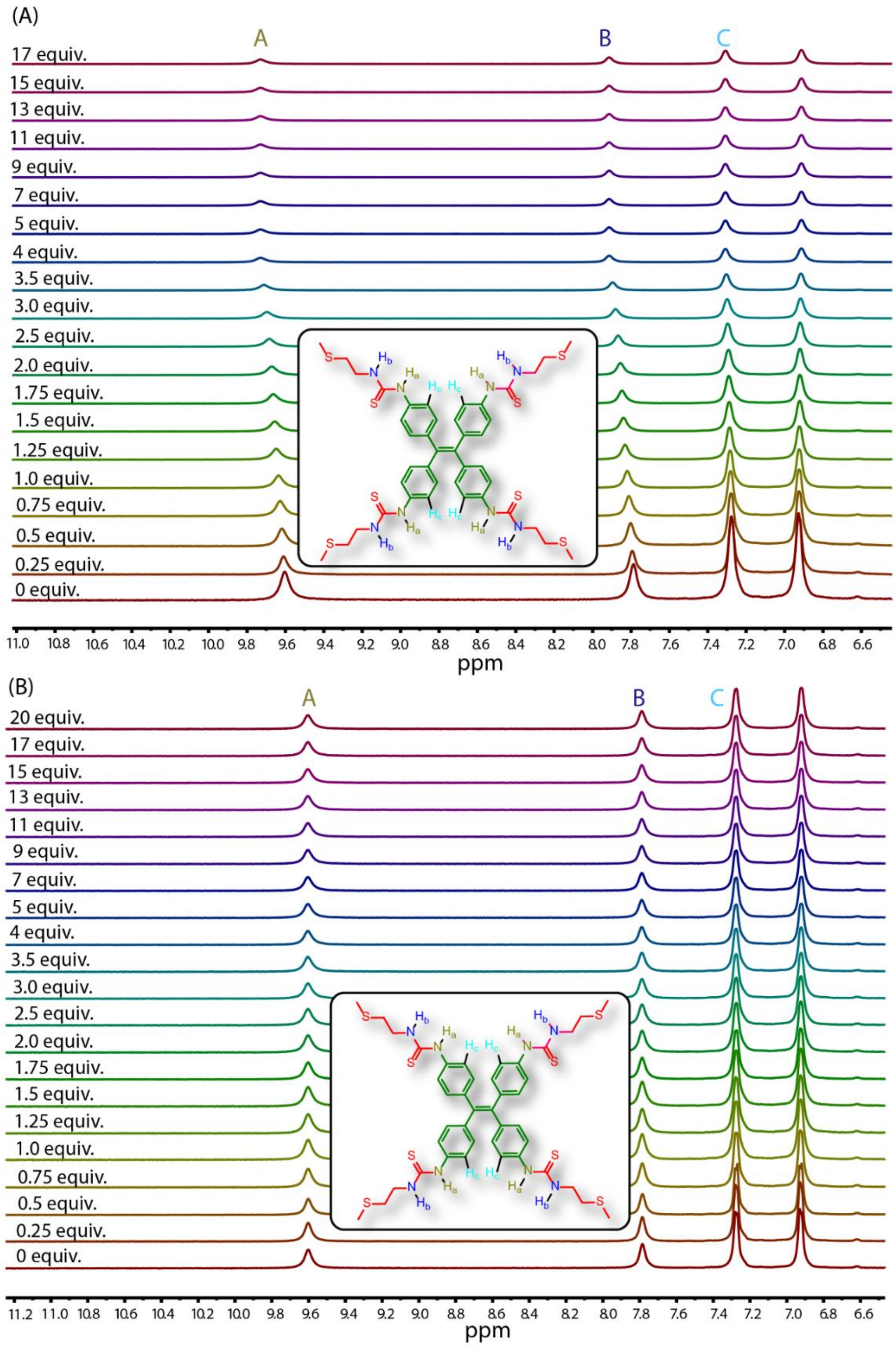

Fig. S9 ^{1}H-NMR (600MHz) titration spectra for compound **1d** with the chronological addition of TBABr (A) and TBAI (B) in DMSO-d_6 solvent, respectively. The amounts of added TBABr and TBAI were shown on the spectra. An insignificant extent of the chemical shift was observed.

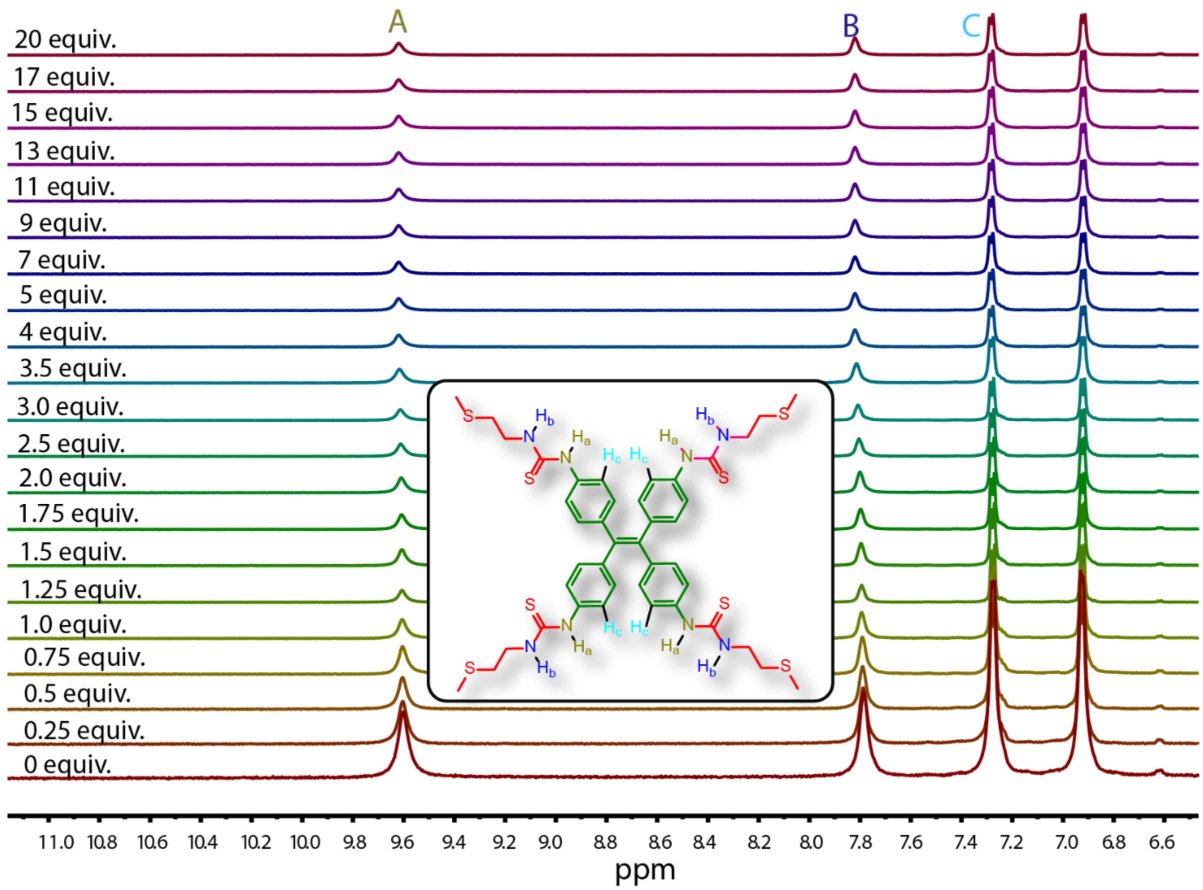

Fig. S10 ^{1}H-NMR (600MHz) titration spectra for compound **1d** with the chronological addition of $TBANO_3$ (A). The amounts of added $TBANO_3$ were shown on the spectra. An insignificant extent of the chemical shift was observed.

3. Density functional theory studies:

Table S2. Optimized structure of compound **1d** using the using B3LYP/ 6-31+G (d) and B3LYP/ 6-31++G (d,p) basic sets.

<table>
<tr><td colspan="2">1d; B3LYP/ 6-31+G (d)</td></tr>
<tr><td>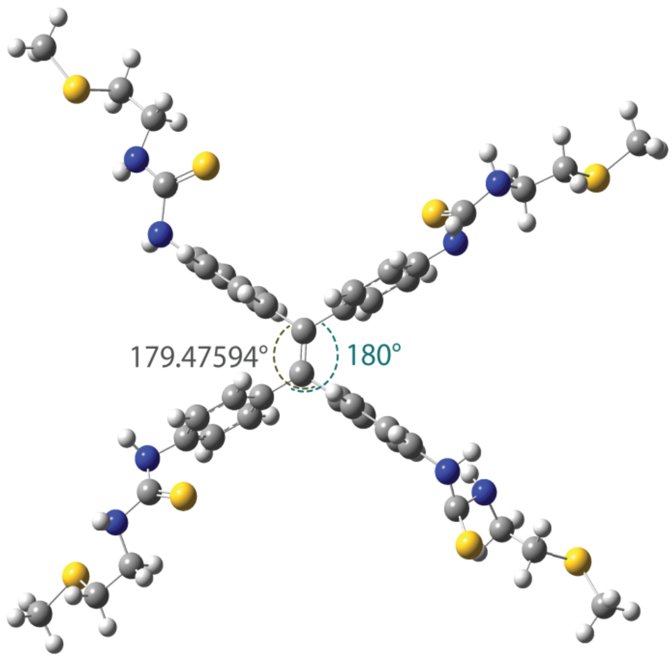
</td><td>Optimized Energy (a.u)

-5254.85514260</td></tr>
<tr><td>1d; B3LYP/ 6-31++G (d,p)</td><td></td></tr>
<tr><td>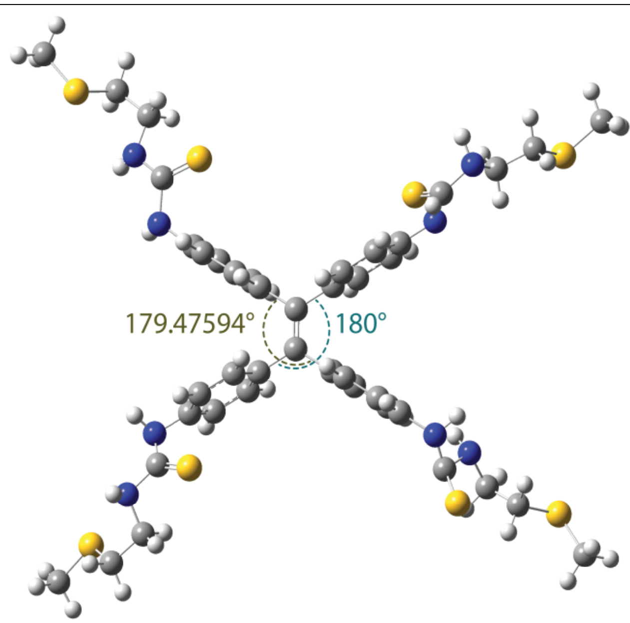
</td><td>Optimized Energy (a.u)

-5254.94950766</td></tr>
</table>

Table S3. XYZ Cartesian coordinate for compound '**1d---Cl$^-$ complex**' using B3LYP/ 6-31+G (d) and B3LYP/ 6-31++G (d,p) basic sets.

1d---Cl$^-$ { (B3LYP/ 6-31+G (d) basic set}				**1d**---Cl$^-$ { (B3LYP/ 6-31++G (d,p) basic set}			
Total Energy = -7095. 460848 Hartree Imaginary Frequency = 0				Total Energy = -7095.560816 Hartree Imaginary Frequency = 0			
Atom	X	Y	Z	Atom	X	Y	Z
C	-0.280605	0.472282	0.506758	C	-0.28061	0.472282	0.506758
C	-0.274936	-0.86771	0.50743	C	-0.27494	-0.86771	0.50743
C	-1.596381	1.236604	0.269807	C	-1.59638	1.236604	0.269807
C	-2.421745	1.582429	1.312236	C	-2.42175	1.582429	1.312236
C	-1.949324	1.583617	-1.05731	C	-1.94932	1.583617	-1.05731
C	-3.588658	2.263758	1.066673	C	-3.58866	2.263758	1.066673
H	-2.139887	1.309255	2.339405	H	-2.13989	1.309255	2.339405
C	-3.137006	2.275676	-1.29396	C	-3.13701	2.275676	-1.29396
H	-1.294576	1.311183	-1.89788	H	-1.29458	1.311183	-1.89788
C	-3.976151	2.625019	-0.21521	C	-3.97615	2.625019	-0.21521
H	-4.230318	2.52675	1.920108	H	-4.23032	2.52675	1.920108
H	-3.419464	2.54873	-2.32107	H	-3.41946	2.54873	-2.32107
C	1.04295	-1.63203	0.732365	C	1.04295	-1.63203	0.732365
C	1.540279	-1.9827	1.895773	C	1.540279	-1.9827	1.895773
C	1.776663	-1.97415	-0.5088	C	1.776663	-1.97415	-0.5088
C	2.74581	-2.67532	2.011694	C	2.74581	-2.67532	2.011694
H	0.972045	-1.71336	2.797833	H	0.972045	-1.71336	2.797833
C	2.982148	-2.66619	-0.39296	C	2.982148	-2.66619	-0.39296
H	1.394259	-1.69788	-1.50224	H	1.394259	-1.69788	-1.50224
C	3.467017	-3.01656	0.867736	C	3.467017	-3.01656	0.867736
H	3.12784	-2.95097	3.005331	H	3.12784	-2.95097	3.005331
H	3.550939	-2.9354	-1.29479	H	3.550939	-2.9354	-1.29479
C	1.021672	1.247935	0.778858	C	1.021672	1.247935	0.778858

C	1.827778	1.640118	-0.30354	C	1.827778	1.640118	-0.30354
C	1.401941	1.55883	2.073428	C	1.401941	1.55883	2.073428
C	3.009625	2.343013	-0.06765	C	3.009625	2.343013	-0.06765
H	1.52988	1.39541	-1.33336	H	1.52988	1.39541	-1.33336
C	2.583732	2.261139	2.309372	C	2.583732	2.261139	2.309372
H	0.767877	1.249843	2.917208	H	0.767877	1.249843	2.917208
C	3.387984	2.653027	1.238474	C	3.387984	2.653027	1.238474
H	3.643392	2.651385	-0.91174	H	3.643392	2.651385	-0.91174
H	2.882229	2.505739	3.339112	H	2.882229	2.505739	3.339112
C	-1.577212	-1.64336	0.23533	C	-1.57721	-1.64336	0.23533
C	-2.399684	-1.84642	1.504057	C	-2.39968	-1.84642	1.504057
C	-1.998474	-2.14256	-0.86011	C	-1.99847	-2.14256	-0.86011
C	-3.599473	-2.54897	1.388322	C	-3.59947	-2.54897	1.388322
H	-2.085219	-1.45272	2.48143	H	-2.08522	-1.45272	2.48143
C	-3.197732	-2.84537	-0.9758	C	-3.19773	-2.84537	-0.9758
H	-1.367328	-1.98197	-1.7463	H	-1.36733	-1.98197	-1.7463
C	-3.998285	-3.04892	0.148876	C	-3.99829	-3.04892	0.148876
H	-4.229957	-2.70954	2.27486	H	-4.22996	-2.70954	2.27486
H	-3.512416	-3.2396	-1.95296	H	-3.51242	-3.2396	-1.95296
N	4.739687	-3.77084	0.990829	N	4.739687	-3.77084	0.990829
H	5.514413	-3.13347	1.016642	H	5.514413	-3.13347	1.016642
C	5.070263	-4.83802	0.360004	C	5.070263	-4.83802	0.360004
S	5.59424	-6.07846	1.147632	S	5.59424	-6.07846	1.147632
N	5.89716	-4.1809	-0.5109	N	5.89716	-4.1809	-0.5109
H	5.348401	-3.5598	-1.07677	H	5.348401	-3.5598	-1.07677
C	6.491695	-5.21613	-1.36865	C	6.491695	-5.21613	-1.36865
H	6.863222	-4.76611	-2.26551	H	6.863222	-4.76611	-2.26551
H	5.747924	-5.94429	-1.61661	H	5.747924	-5.94429	-1.61661
N	-5.249959	3.395685	-0.42651	N	-5.24996	3.395685	-0.42651
H	-5.620373	3.219883	-1.34248	H	-5.62037	3.219883	-1.34248

C	-5.148814	4.925089	-0.20873	C	-5.14881	4.925089	-0.20873
S	-3.809923	5.517047	0.330301	S	-3.80992	5.517047	0.330301
N	-6.165809	5.696477	-0.38384	N	-6.16581	5.696477	-0.38384
H	-6.67892	5.383281	-1.18742	H	-6.67892	5.383281	-1.18742
C	-5.691704	7.071241	-0.59866	C	-5.6917	7.071241	-0.59866
H	-5.325848	7.470636	0.324129	H	-5.32585	7.470636	0.324129
H	-4.904155	7.067839	-1.32299	H	-4.90416	7.067839	-1.32299
C	-6.855061	7.941538	-1.10933	C	-6.85506	7.941538	-1.10933
H	-6.547339	8.965869	-1.14024	H	-6.54734	8.965869	-1.14024
H	-7.134037	7.623126	-2.09202	H	-7.13404	7.623126	-2.09202
S	-8.247537	7.773138	-0.0134	S	-8.24754	7.773138	-0.0134
C	-9.423791	9.067565	-0.34398	C	-9.42379	9.067565	-0.34398
H	10.285729	8.933006	0.27558	H	-10.2857	8.933006	0.27558
H	-8.977814	10.0171	-0.13328	H	-8.97781	10.0171	-0.13328
H	-9.714903	9.030705	-1.37296	H	-9.7149	9.030705	-1.37296
N	-5.252187	-3.7418	0.055707	N	-5.25219	-3.7418	0.055707
H	-5.940861	-3.20059	0.545531	H	-5.94086	-3.20059	0.545531
C	-5.092158	-4.86259	0.662335	C	-5.09216	-4.86259	0.662335
S	-3.900077	-5.06382	1.648262	S	-3.90008	-5.06382	1.648262
N	-6.16081	-5.86801	0.586896	N	-6.16081	-5.86801	0.586896
H	-6.591614	-5.96588	1.487974	H	-6.59161	-5.96588	1.487974
C	-5.590483	-7.15831	0.173691	C	-5.59048	-7.15831	0.173691
H	-5.09541	-7.61251	1.006463	H	-5.09541	-7.61251	1.006463
H	-4.886845	-7.00049	-0.61681	H	-4.88685	-7.00049	-0.61681
C	-6.718247	-8.0835	-0.32004	C	-6.71825	-8.0835	-0.32004
H	-6.306146	-9.03086	-0.5986	H	-6.30615	-9.03086	-0.5986
H	-7.434184	-8.22233	0.462948	H	-7.43418	-8.22233	0.462948
S	-7.516316	-7.34598	-1.72984	S	-7.51632	-7.34598	-1.72984
C	-8.681603	-8.49892	-2.42354	C	-8.6816	-8.49892	-2.42354
H	-9.166267	-8.05249	-3.26657	H	-9.16627	-8.05249	-3.26657
H	-8.165945	-9.38305	-2.7355	H	-8.16595	-9.38305	-2.7355

H	-9.413078	-8.7543	-1.68555	H	-9.41308	-8.7543	-1.68555
C	7.650295	-5.90032	-0.61957	C	7.650295	-5.90032	-0.61957
H	7.340262	-6.87113	-0.29351	H	7.340262	-6.87113	-0.29351
H	7.924317	-5.30957	0.229442	H	7.924317	-5.30957	0.229442
S	9.049359	-6.05891	-1.70855	S	9.049359	-6.05891	-1.70855
C	10.020478	-7.47064	-1.22652	C	10.02048	-7.47064	-1.22652
H	9.437927	-8.36065	-1.3424	H	9.437927	-8.36065	-1.3424
H	10.891945	-7.53183	-1.84434	H	10.89195	-7.53183	-1.84434
H	10.315325	-7.36808	-0.20308	H	10.31533	-7.36808	-0.20308
N	4.633887	3.392542	1.486954	N	4.633887	3.392542	1.486954
H	4.599328	3.809169	2.399281	H	4.599328	3.809169	2.399281
C	4.789265	4.445475	0.473007	C	4.789265	4.445475	0.473007
N	5.883664	5.420959	0.580814	N	5.883664	5.420959	0.580814
H	5.50265	6.333815	0.750038	H	5.50265	6.333815	0.750038
S	3.78522	4.528287	-0.72643	S	3.78522	4.528287	-0.72643
C	6.65239	5.435392	-0.67208	C	6.65239	5.435392	-0.67208
H	6.112721	5.984221	-1.41535	H	6.112721	5.984221	-1.41535
H	6.803215	4.431276	-1.00958	H	6.803215	4.431276	-1.00958
C	8.017366	6.105783	-0.42915	C	8.017366	6.105783	-0.42915
H	7.867277	7.121185	-0.12694	H	7.867277	7.121185	-0.12694
H	8.541821	5.578496	0.340144	H	8.541821	5.578496	0.340144
S	8.972286	6.068646	-1.93087	S	8.972286	6.068646	-1.93087
C	10.319456	7.225459	-1.80711	C	10.31946	7.225459	-1.80711
H	10.936666	7.148635	-2.67777	H	10.93667	7.148635	-2.67777
H	9.930355	8.219394	-1.73232	H	9.930355	8.219394	-1.73232
H	10.901164	7.003737	-0.93685	H	10.90116	7.003737	-0.93685
Cl	-7.753512	-4.33365	0.740831	Cl	-7.75351	-4.33365	0.740831
Cl	-7.714784	3.572063	-1.18294	Cl	-7.71478	3.572063	-1.18294
Cl	6.099755	-1.72971	-0.45231	Cl	6.099755	-1.72971	-0.45231
Cl	6.386077	4.715264	2.416044	Cl	6.386077	4.715264	2.416044

4. Ion transporting activity studies:

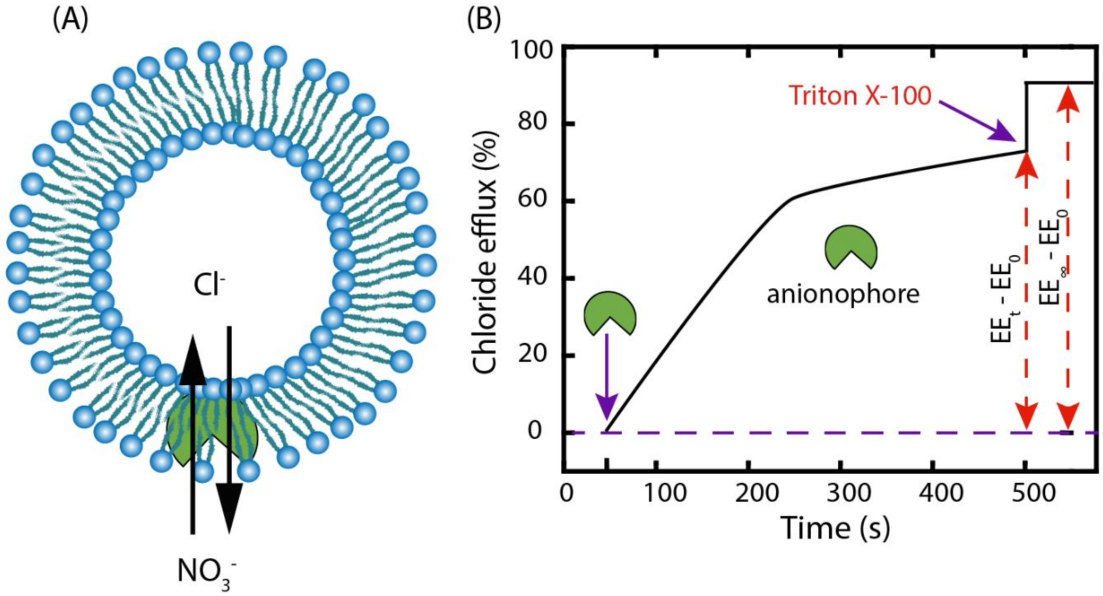

Fig. S11 Representations of chloride efflux study across the EYPC/CHOL-LUVs (A and B).

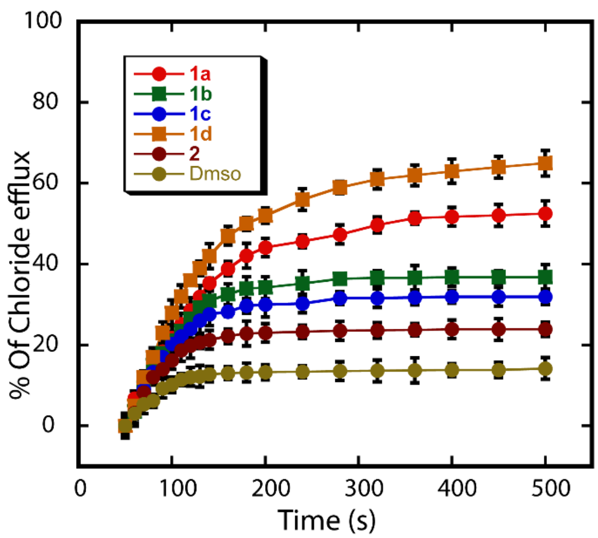

Fig. S12 Initial screening for the compound-mediated transmembrane transport of Cl^- ions (at concentration 0.156 μM).

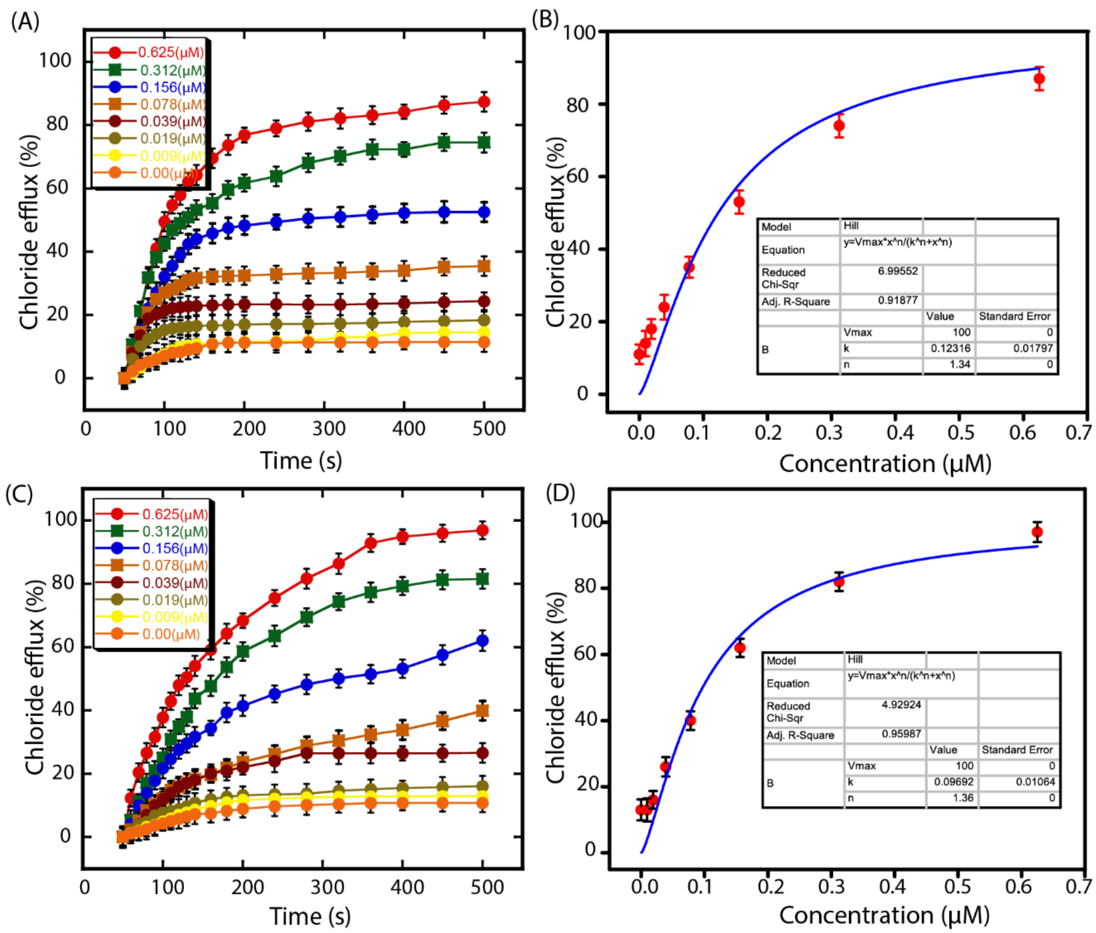

Fig. S13 Concentration-dependent Cl^{-} ion transport activity of compounds **1a** (A and B) and **1d** (C and D) were measured by chloride ion-selective electrode using EYPC/CHOL-LUVs at pH 7.2.

Cation selectivity studies were also performed by the ISE based assay as described above using EYPC/CHOL-LUVs, where 5 mM phosphate buffer, pH 7.2 containing 100 mM MCl salt (where M = Li^+ , Na^+ , K^+ , Rb^+, and Cs^+) was used as a intravesicular medium and extravesicular medium was filled with 5 mM phosphate buffer, pH 7.2, containing 100 mM $NaNO_3$.

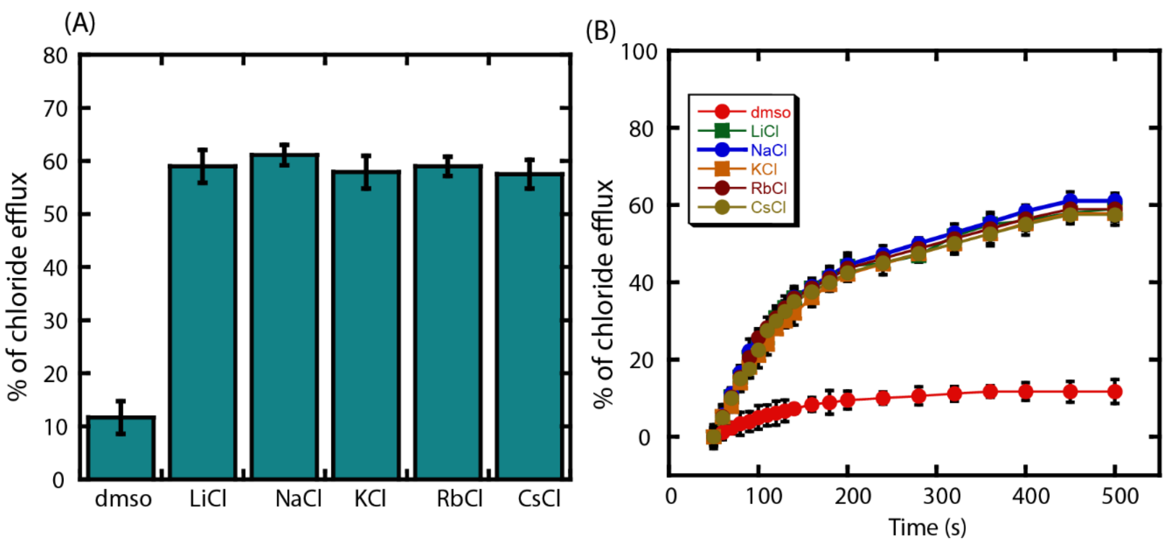

Fig. S14 Chloride ion transport efficiency of the compound **1d** (0.156 μM = 0.05 mol % with respect to lipid) across the EYPC/CHOL-LUVs (6:4 molar ratio) was measured by an ISE-based assay at pH 7.2 in presence of different metal ion to rule out the possibility of metal ion dependency where figure A represents the bar plot and figure B corresponding plot.

Table S4. Cl^- ion transport properties of the compounds.

Compound Code	EC_{50} values (μM)	EC_{50} values (mol %)	Hill coefficient (n)
1a	0.123 ± 0.018	0.039 ± 0.006	1.34
1b	-		-
1c	-		-
1d	0.097 ± 0.011	0.031 ± 0.003	1.36

N.B. EC_{50} values of compounds **1b** and **1c** could not be done due to the precipitation at higher concentrations.

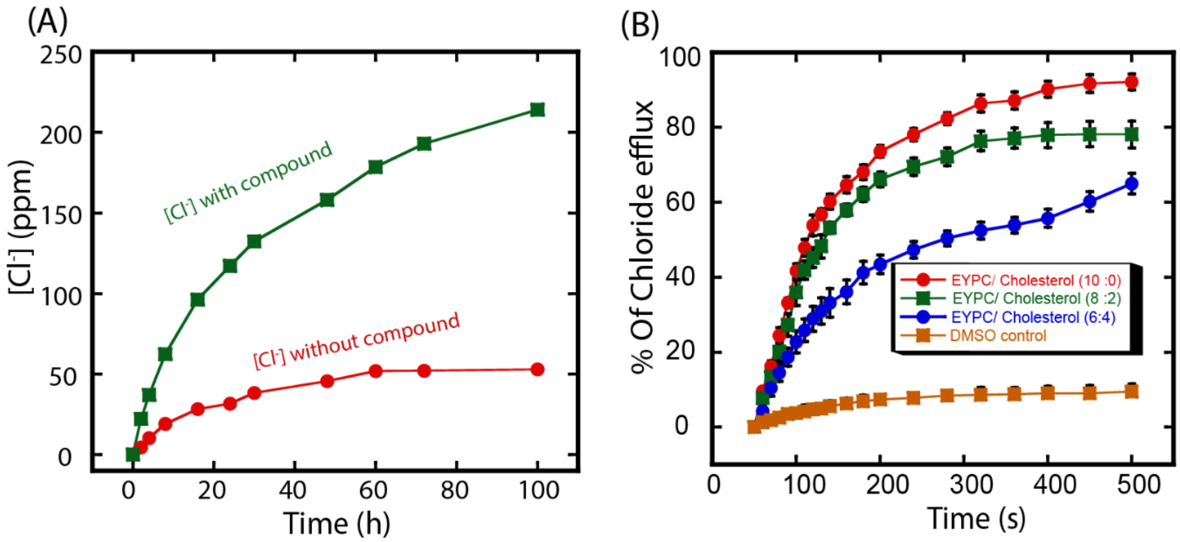

Fig. S15 The probability of Cl^-/ NO_3^- antiport mechanistic pathway of compound **1d** by the U-tube assay in the presence of NaCl at left arm and $NaNO_3$ at right arm (A). Cholesterol-dependent chloride efflux assay using ISE to validate the carrier-mechanistic pathway of Cl^- ion transport activity by the compound **1d** across the different ratios of cholesterol encapsulated EYPC-LUVs (B). Experiment was performed at 0.156 μM = 0.05 mol % with respect to lipid.

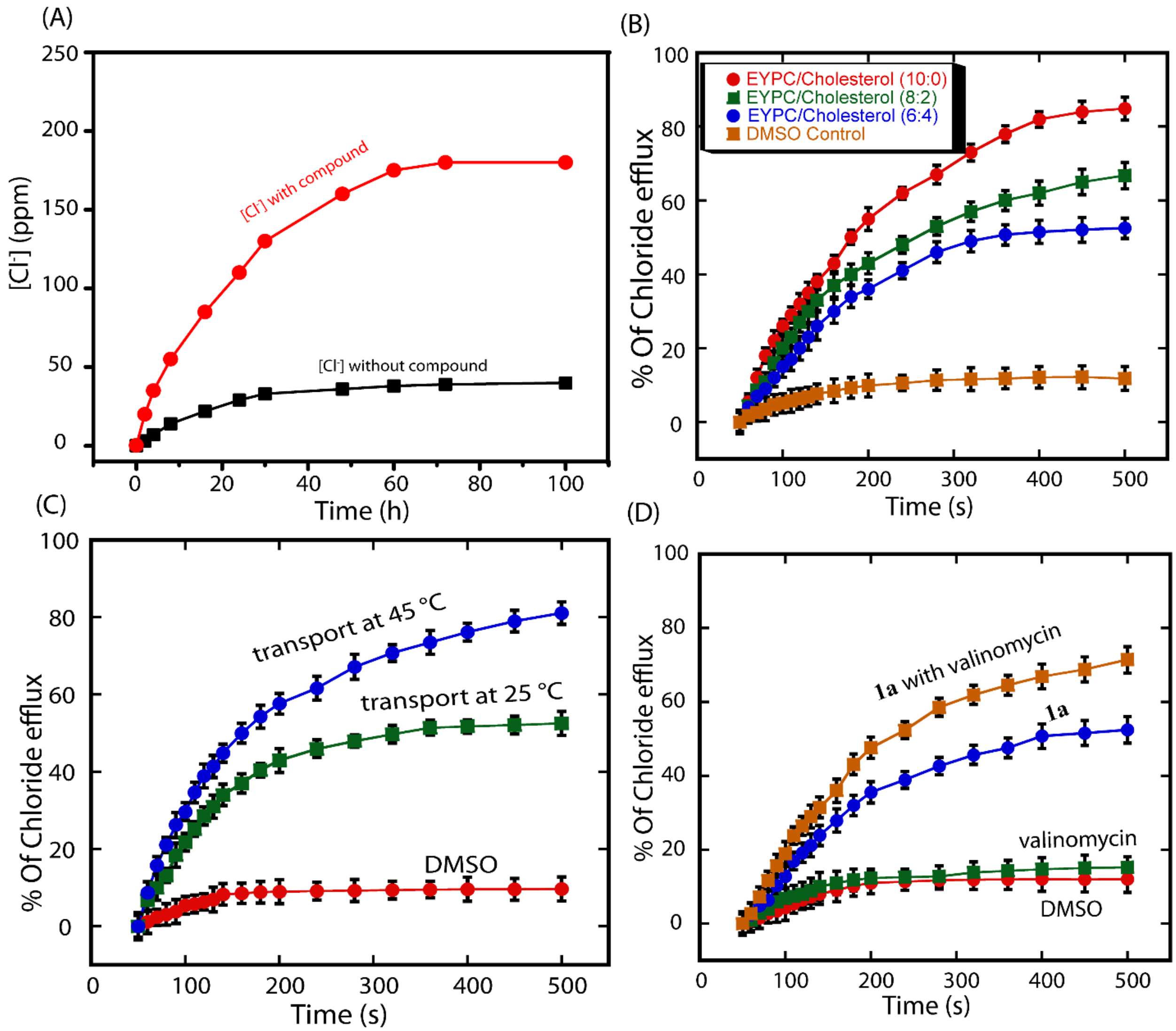

Fig. S16 The probability of Cl-/ NO_3^- antiport mechanistic pathway of compound **1a** by the U-tube assay in the presence of NaCl at left arm and $NaNO_3$ at right arm (A). Cholesterol-dependent chloride efflux assay using ISE to validate the carrier-mechanistic pathway of Cl^- ion transport activity by the compound **1a** across the different ratios of cholesterol encapsulated EYPC-LUVs (B). Cholesterol-dependent chloride efflux assay using ISE to validate the carrier-mechanistic pathway of Cl^- ion transport activity by the compound **1a** across the different ratios of cholesterol encapsulated EYPC-LUVs (C). Experiment was performed at 0.156 µM = 0.05 mol % with respect to lipid. Percentage of Cl^- ion transport activity of compound **1a** in the absence and presence of valinomycin (D).

5. Regeneration of the active compound 1d from its proanionophore 2:

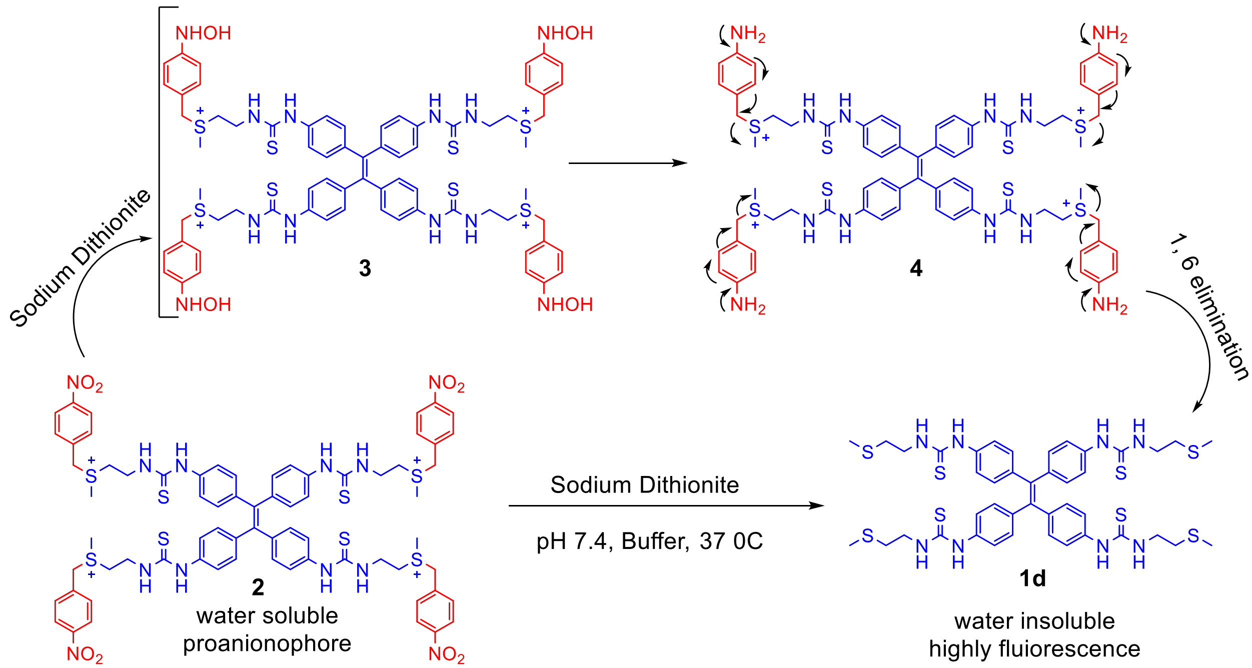

Fig. S17 Regeneration of the active compound in the presence of sodium dithionite.

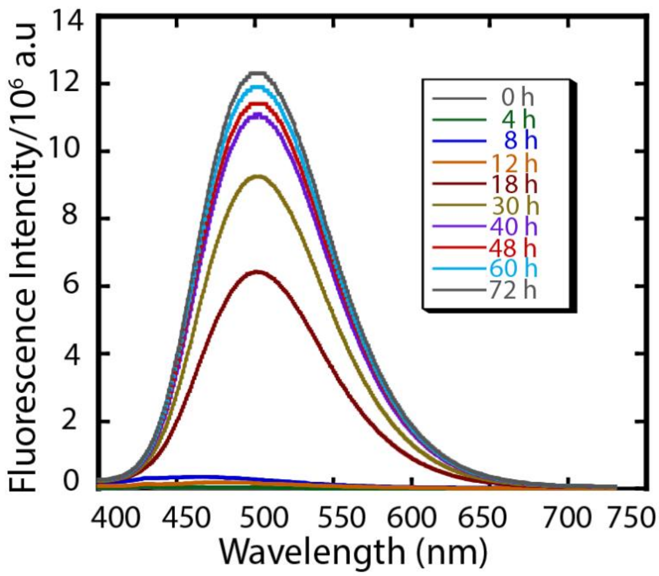

Fig. S18 Regeneration of the active compound **1d** from the proanionophore **2** in the presence of sodium dithionite. The initial concentration of the proanionophore **2** was 1 mM.

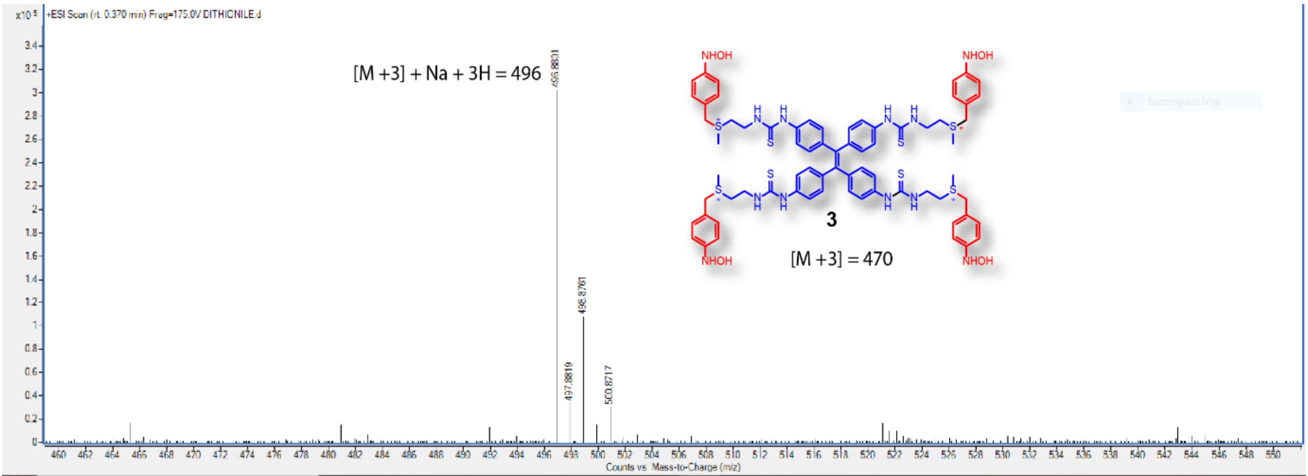

Fig. S19 The reaction of proanionophore **2** in the presence of sodium dithionite in PBS at 37 ºC led to the generation of intermediate compound **3,** which was also confirmed by ES-MS analysis.

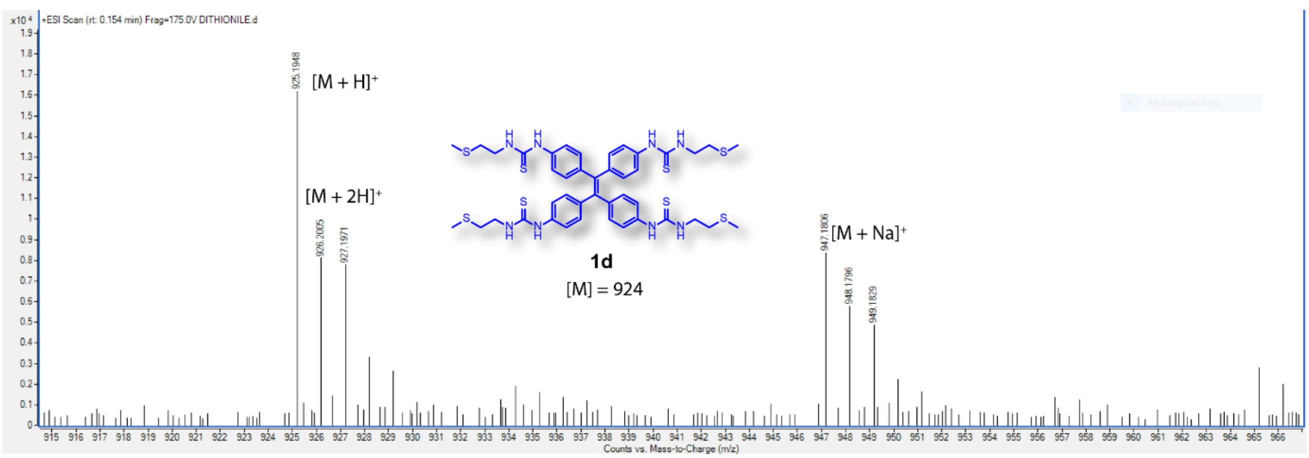

Fig. S20 The reaction of **p**roanionophore **2** in the presence of sodium dithionite in PBS at 37 ºC led to the regeneration of active compound **1d,** which was also confirmed by ES-MS analysis.

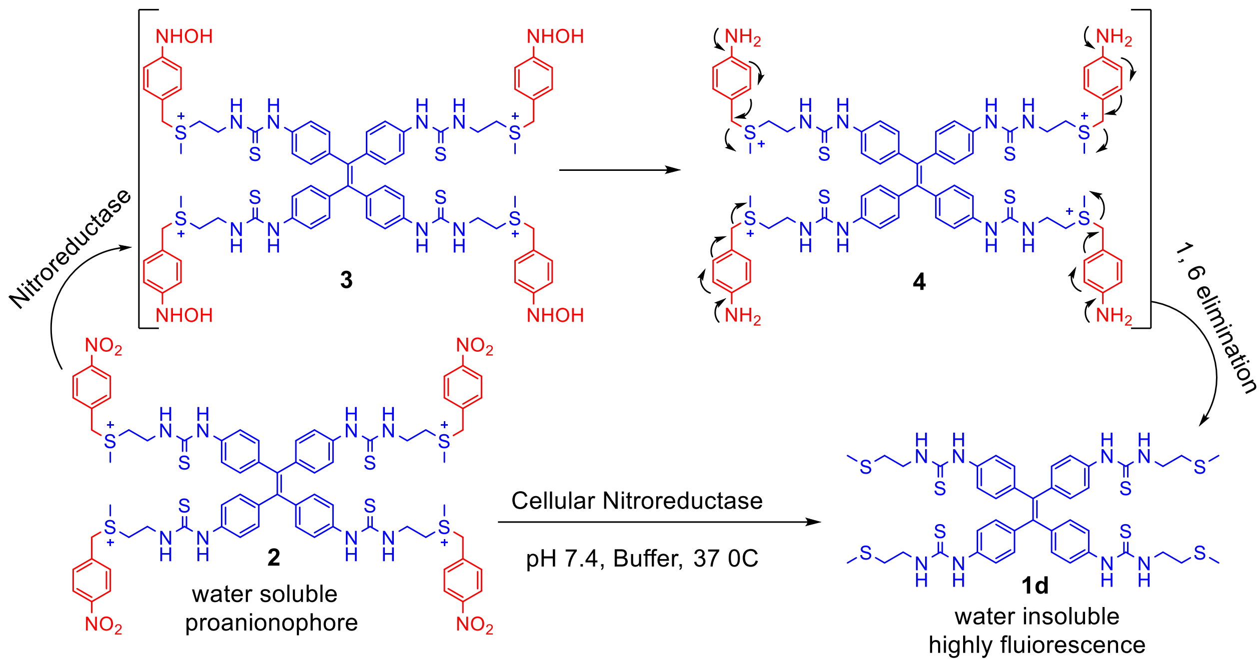

Fig. S21 Regeneration of the active compound in the presence of nitroreductase enzyme (bacterial cellular extract).

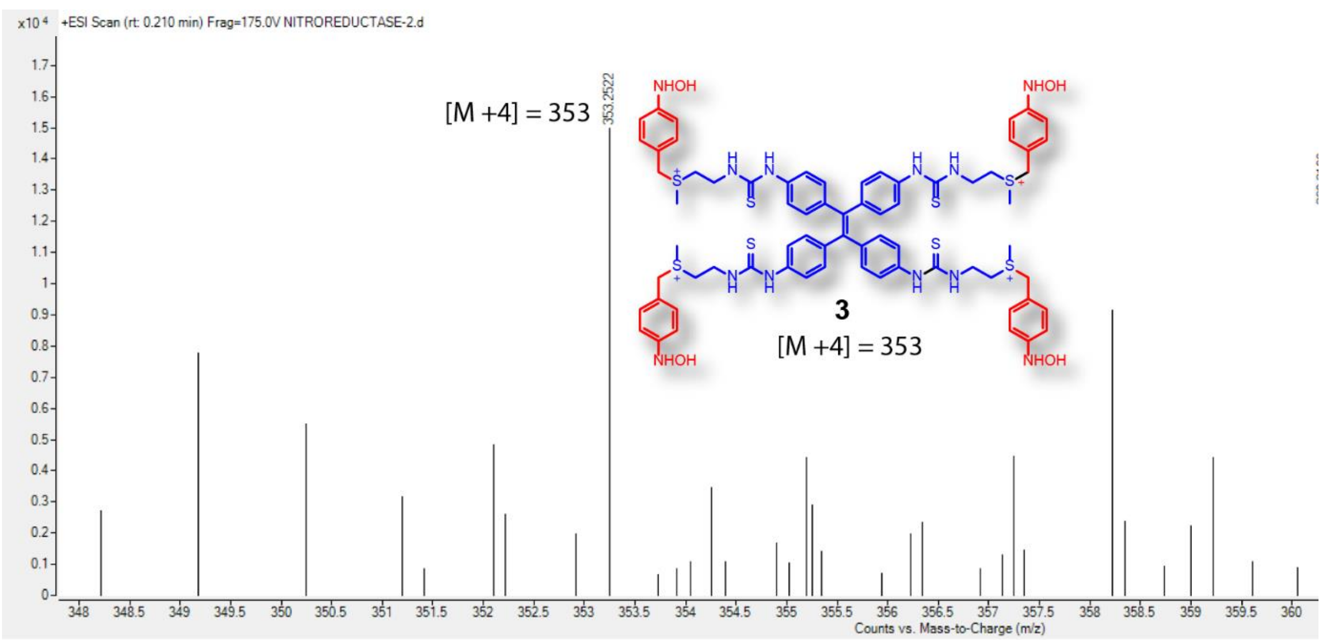

Fig. S22 The reaction of **p**roanionophore **2** in the presence of bacterial cell lysate containing nitroreductase in PBS at 37 ºC led to the generation of intermediate compound **3,** which was also confirmed by ES-MS analysis.

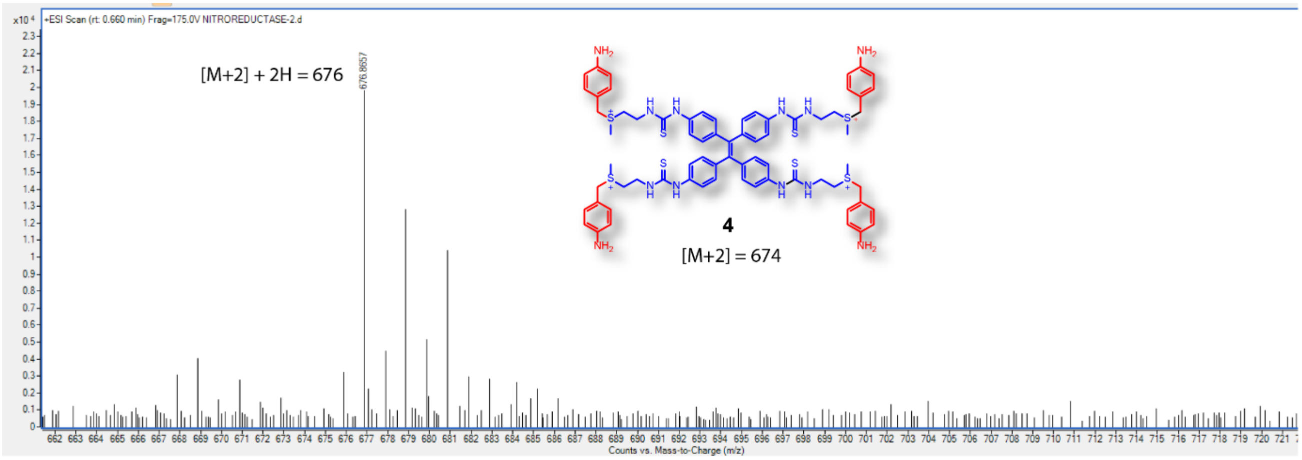

Fig. S23 The reaction of **p**roanionophore **2** in the presence of bacterial cell lysate containing nitroreductase in PBS at 37 ºC led to the generation of intermediate compound **4,** which was also confirmed by ES-MS analysis.

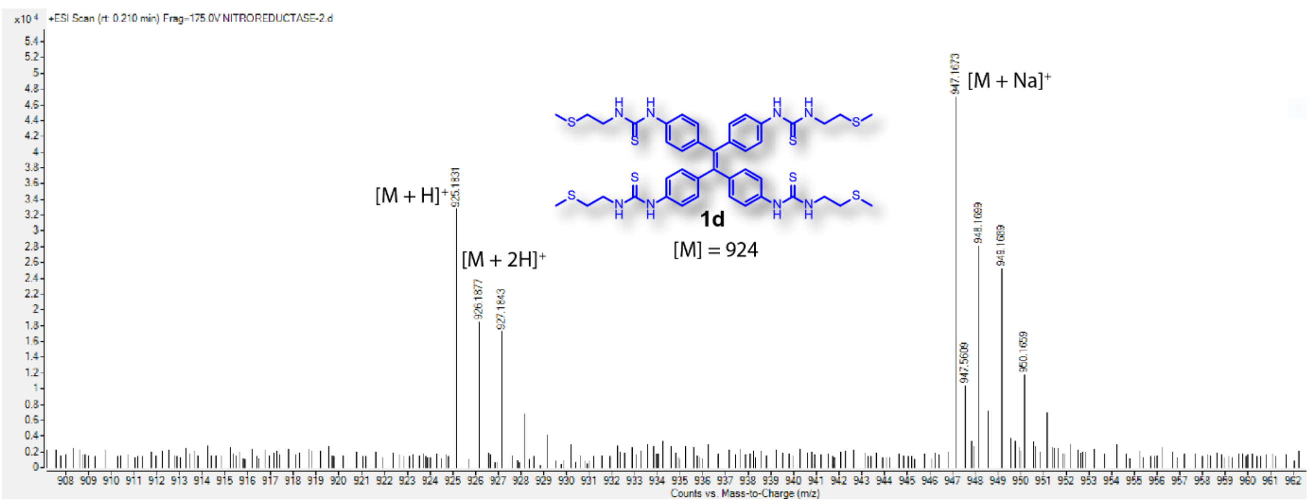

Fig. S24 The reaction of **p**roanionophore **2** in the presence of bacterial cell lysate containing nitroreductase in PBS at 37 ºC led to the regeneration of active anionophore **1d,** which was also confirmed by ES-MS analysis.

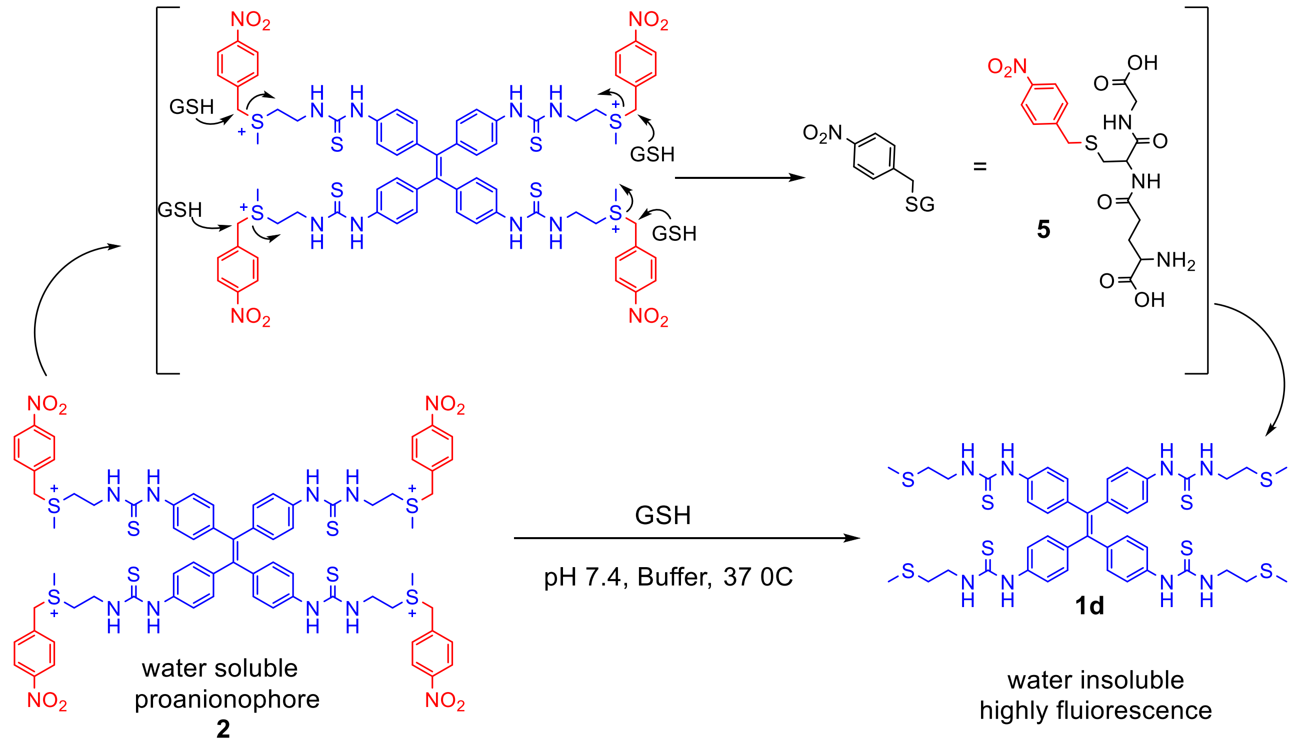

Fig. S25 Regeneration of the active compound in the presence of the GSH.

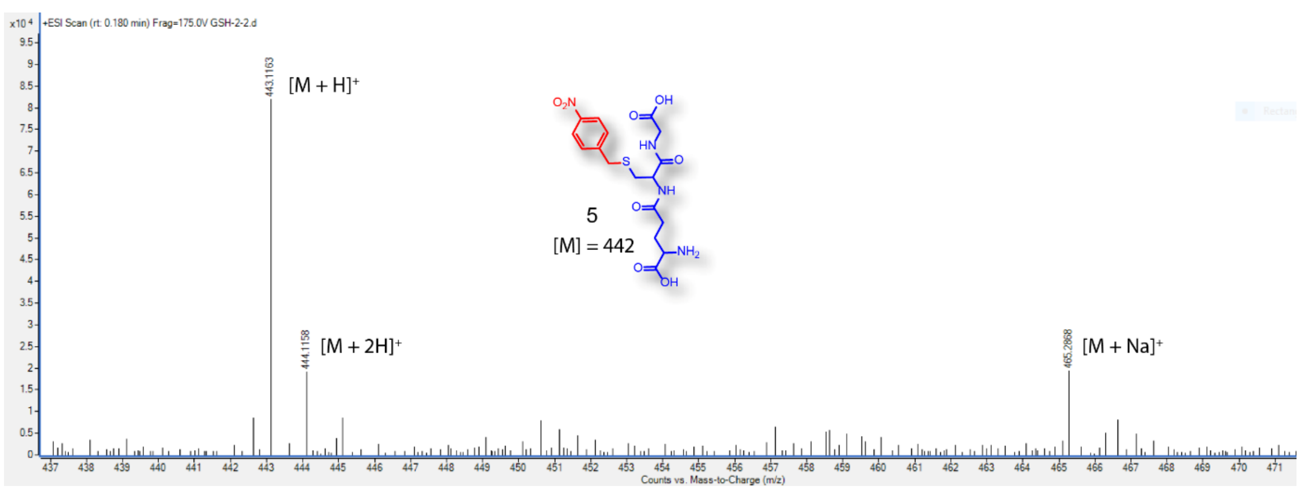

Fig. S26 The reaction of **p**roanionophore **2** in the presence of GSH in PBS at 37 ºC led to the generation of intermediate compound **5**, which was also confirmed by ES-MS analysis.

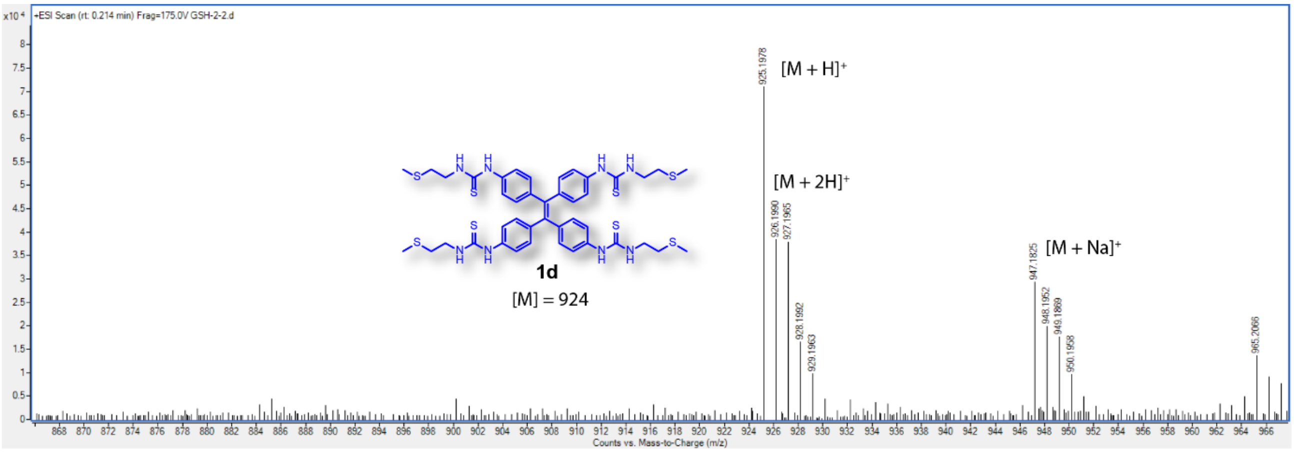

Fig. S27 The reaction of **p**roanionophore **2** in the presence of GSH in PBS at 37 ºC led to the regeneration of active anionophore **1d**, which was also confirmed by ES-MS analysis.

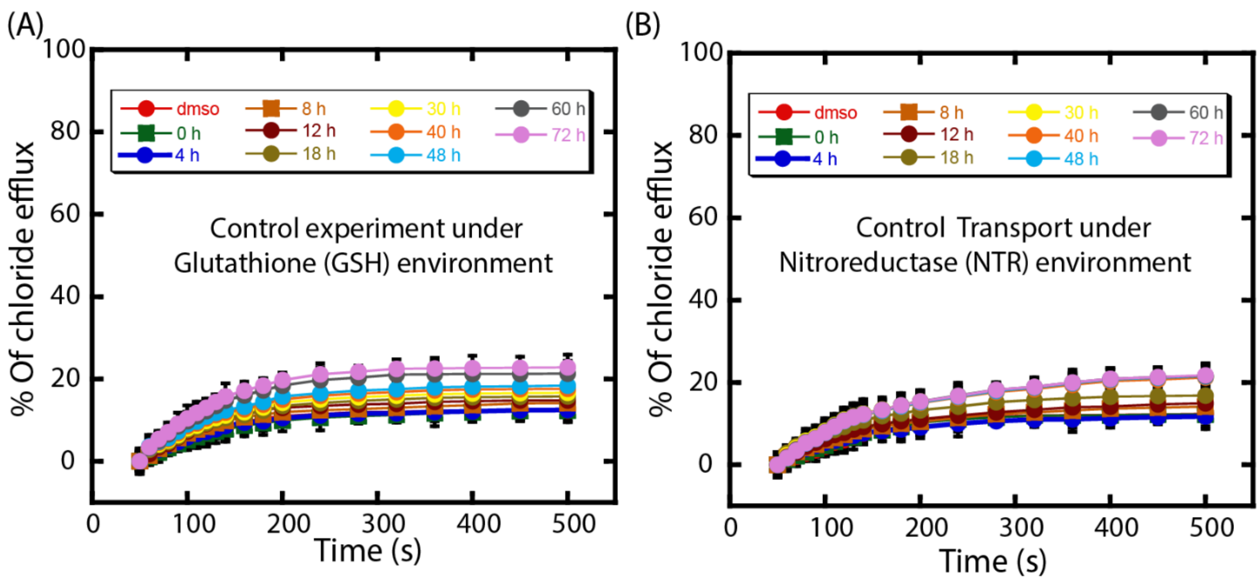

Fig. S28 Control experiments for the Cl^- ion transport activities of active anionophore **1d** from its proanionophore **2** in the presence of GSH (A) and NTR enzyme (B). The concentration of the proanionophore **2** was 1 mM.

6. Transport of chloride ions across the giant unilamellar vesicles:

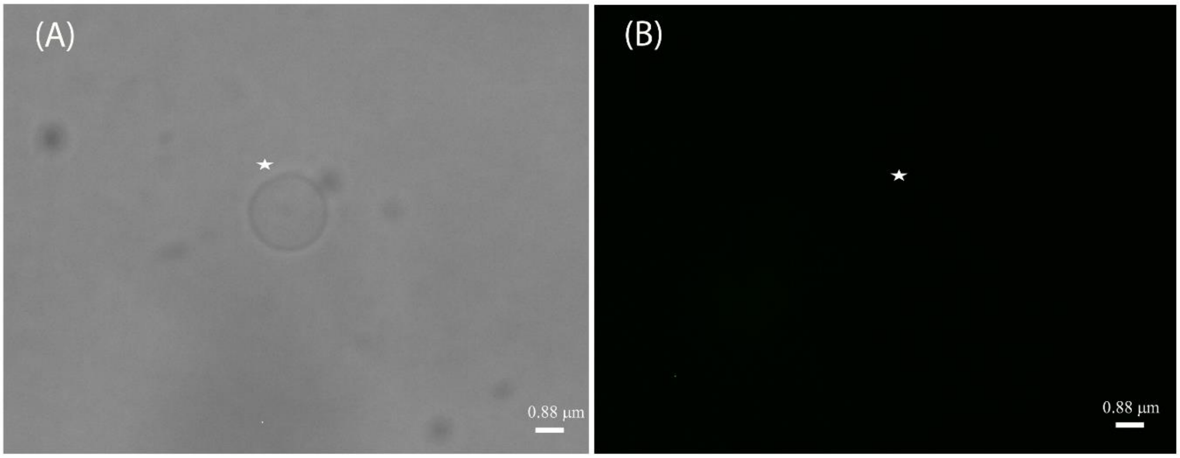

Fig. S29 Fluorescence microscopic images of the compound **1d** (1 μM) loaded GUVs. Bight filed (A) and green channel (B). Microscopic images showed that at this concentration of compound **1d,** the fluorescence intensity in the green channel is not detectable, which ruled out the interference of the fluorescence of the compound during lucigenin encapsulated GUVs assay.

7. Chloride transport by ^{35}Cl NMR measurements:

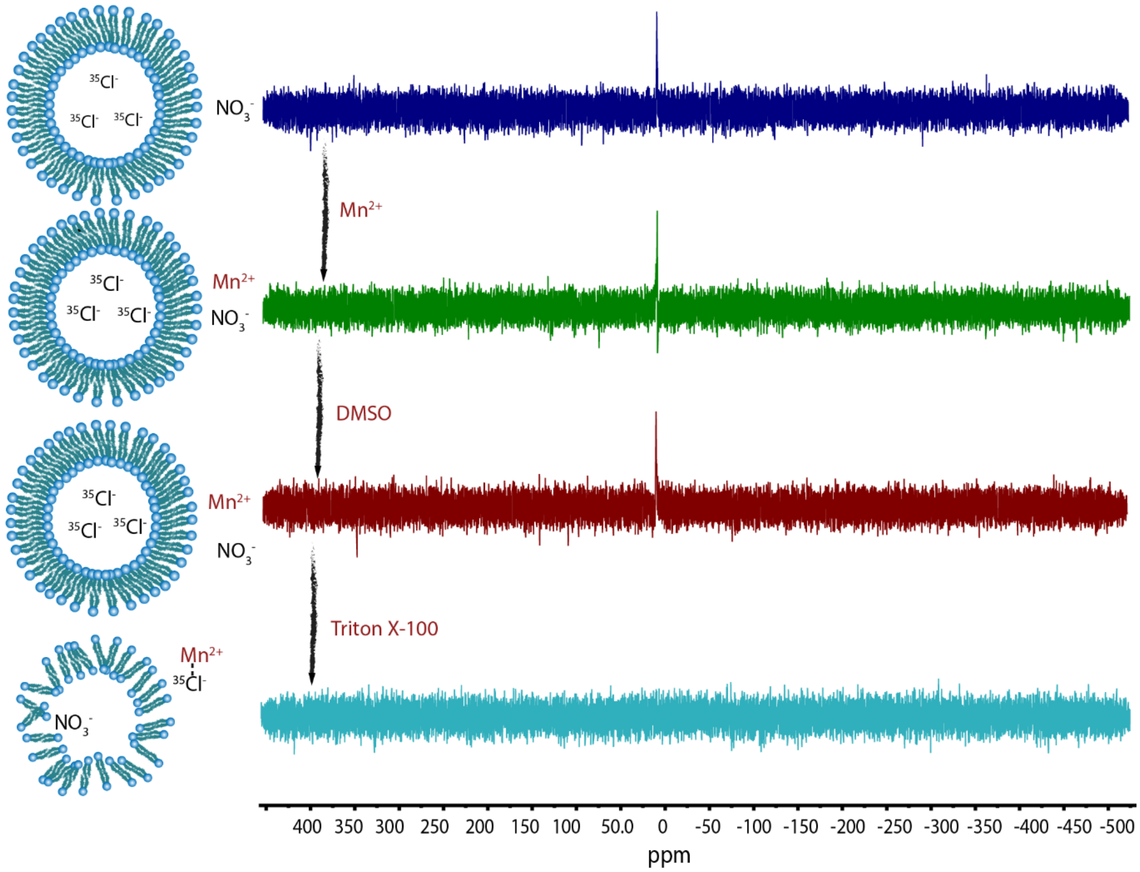

Fig. S30 The ^{35}Cl NMR control experiment was performed in the absence of a compound. The NMR experiment was performed in H_2O: D_2O (9:1) solution.

8. Validation of AIE property:

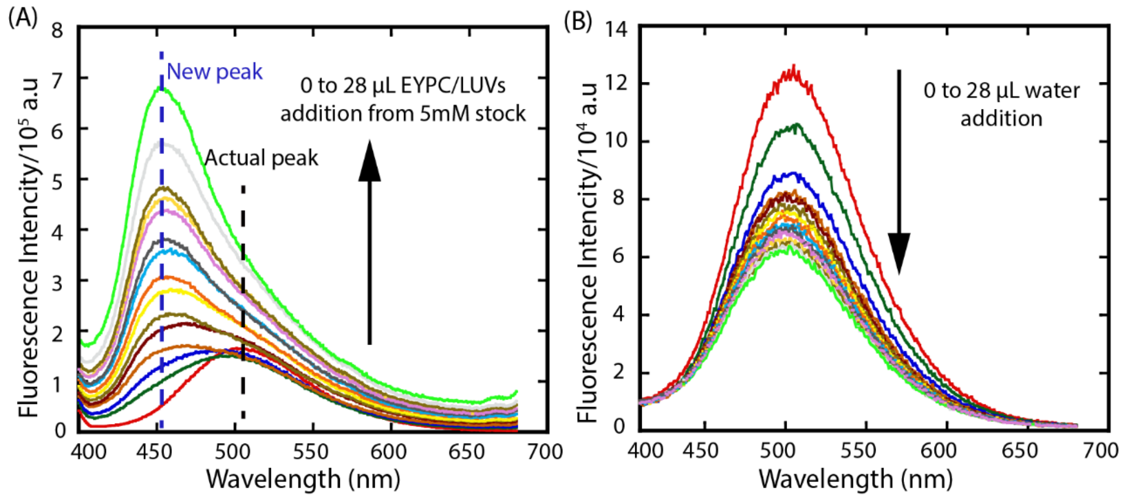

Fig. S31 Fluorescence emission spectra of compound **1d** (0.03 μM) in the presence of the liposomal solution (0 - 28 μL addition of EYPC-LUVs from 5 mM stock), where a clear blue shift with significant fluorescence enhancement was observed (A). The control experiment in the presence of the same amount (0 - 28 μL) of water (B). For both cases, the compound was excited at 350 nm.

9. Staining of GUVs:

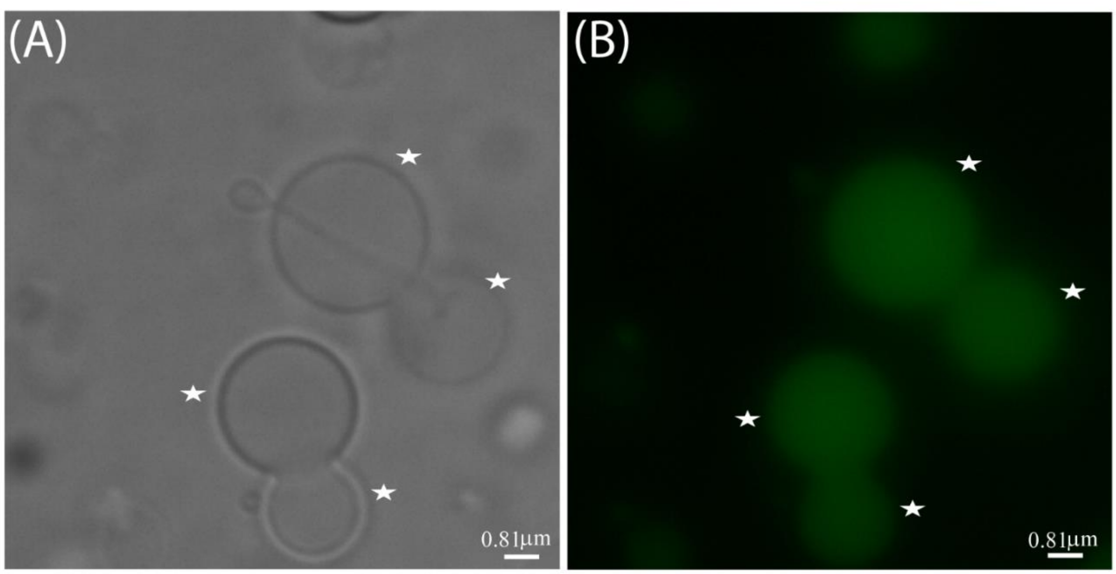

Fig. S32 Fluorescence microscopic images of the compound **1d** (10 μM) loaded GUVs. Bight filed (A) and green channel (B) illustrates the compound **1d** encapsulation efficiency of the GUVs. The scale bar of the images was 0.81 μm.

10. Selectivity of the stimuli:

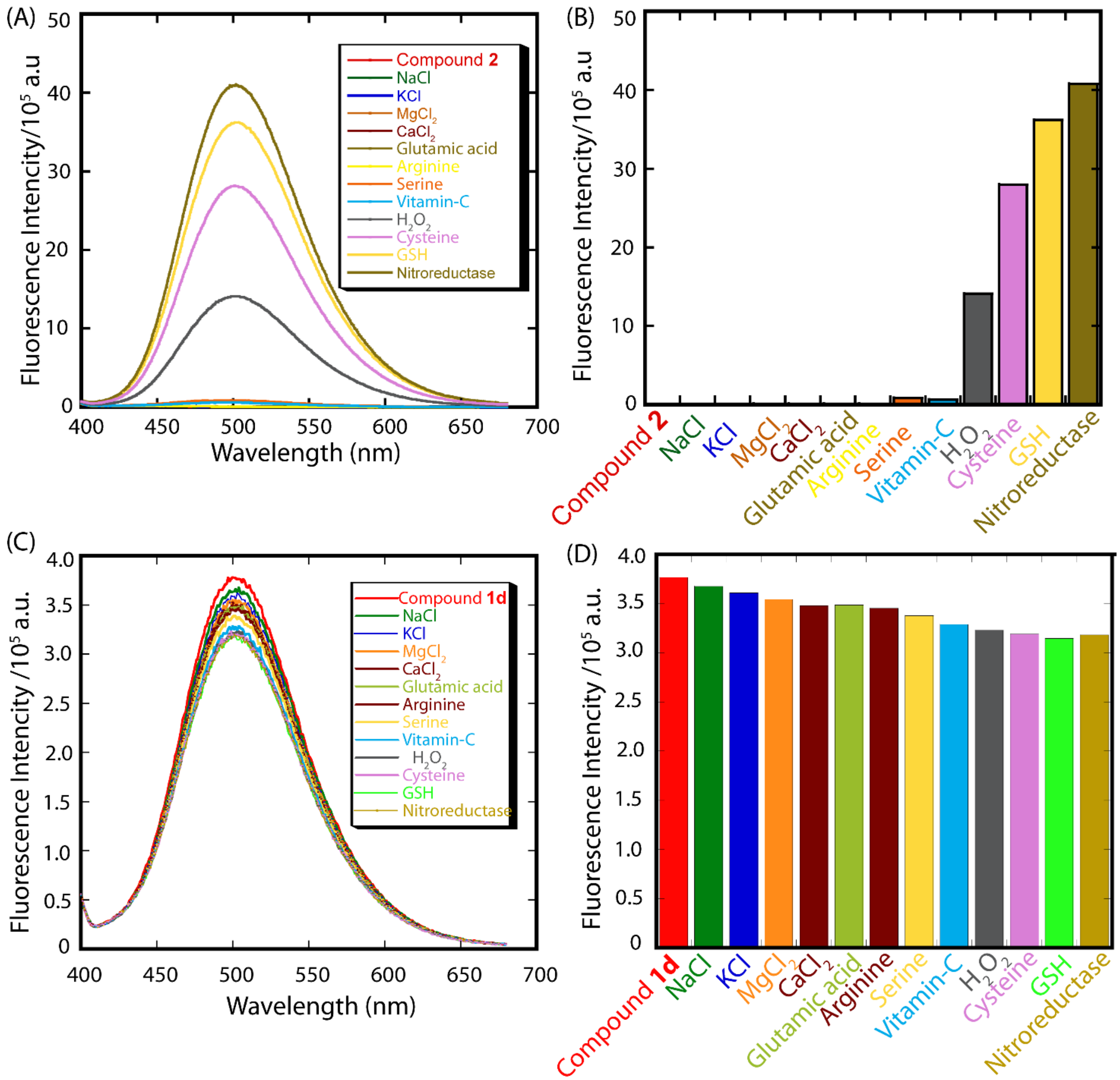

Fig. S33 Regeneration of the active compound **1d** from the proanionophore **2** in the presence of the different substances. Proanionophore **2** and active compound **1d** was (1 mM) were incubated with individual substances (10 mM), and fluorescence spectra were recorded after 72 h of incubation. Fluorescence spectra of proanionophore **2** **(A)** compound **1d** (C) and bar plot diagram of proanionophore **2** **(B)** compound **1d** (D).

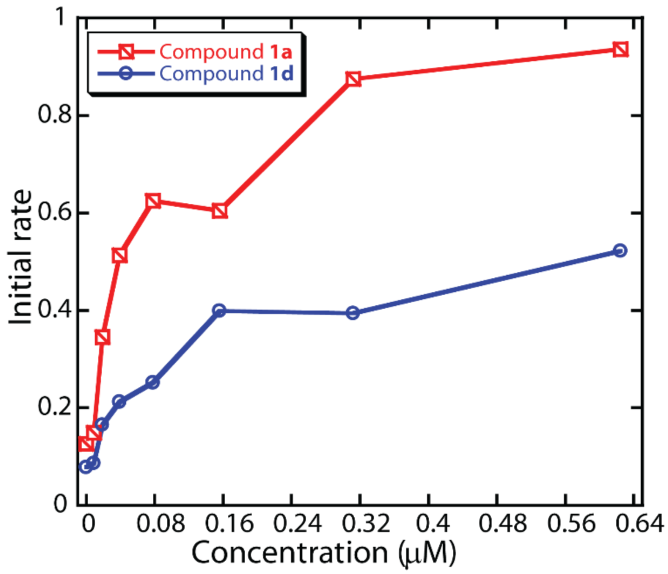

Fig. S34 A plot of the initial rates of Cl^- ion transport activities at different concentrations of compounds**.**

11. NMR spectra of the compounds:

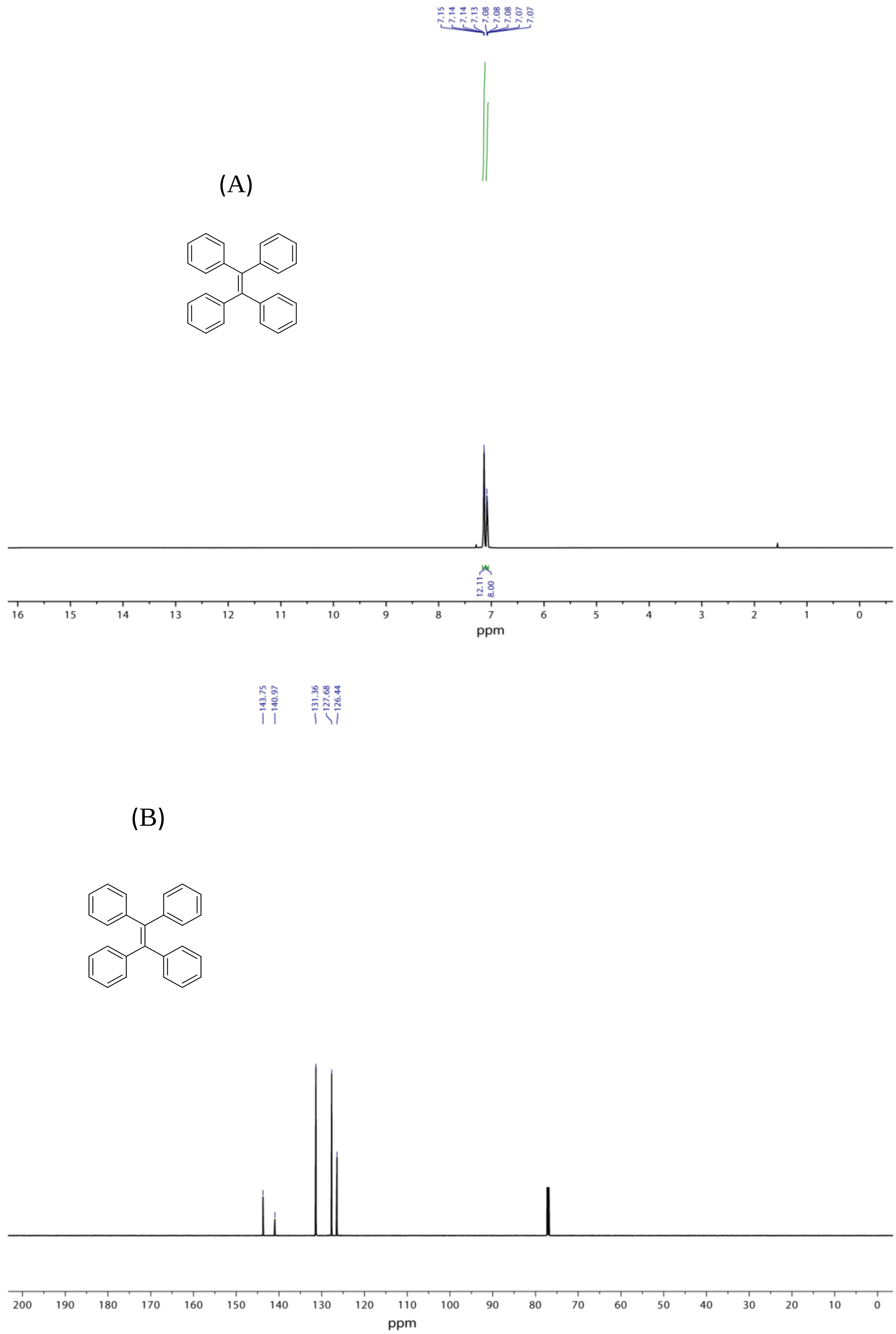

Fig. S35 ^{1}H NMR (A) and ^{13}C NMR (B) spectra of compound **TPE**.

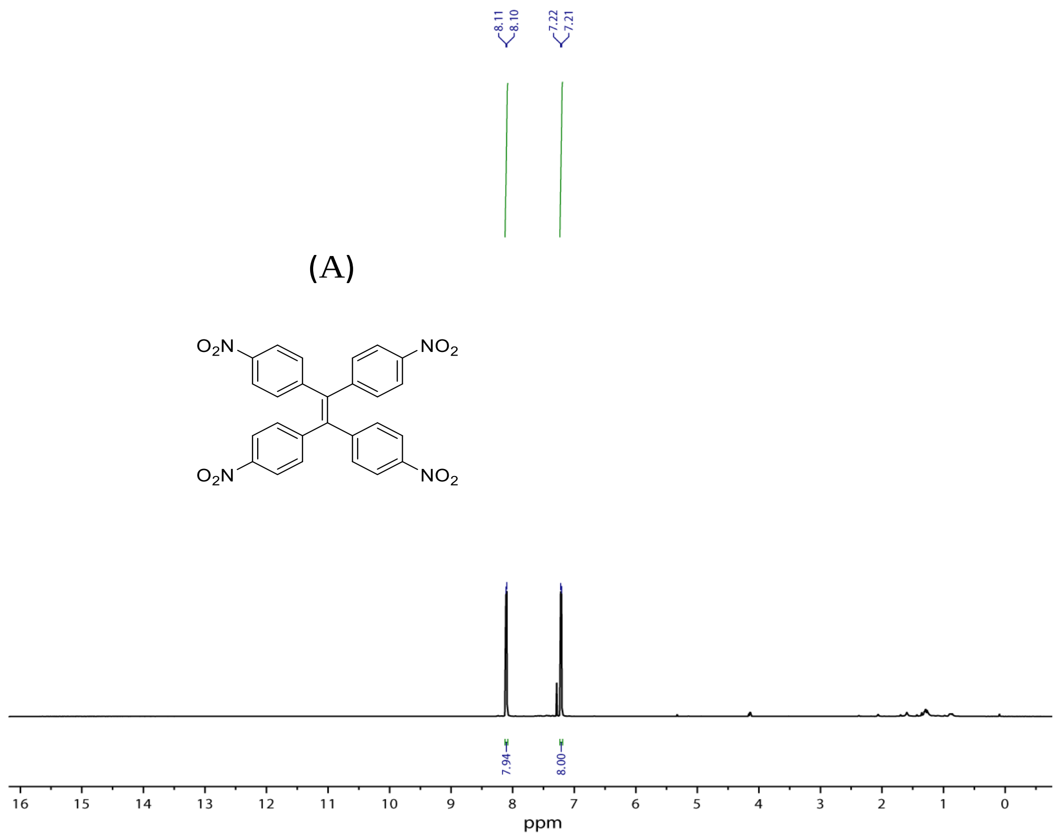

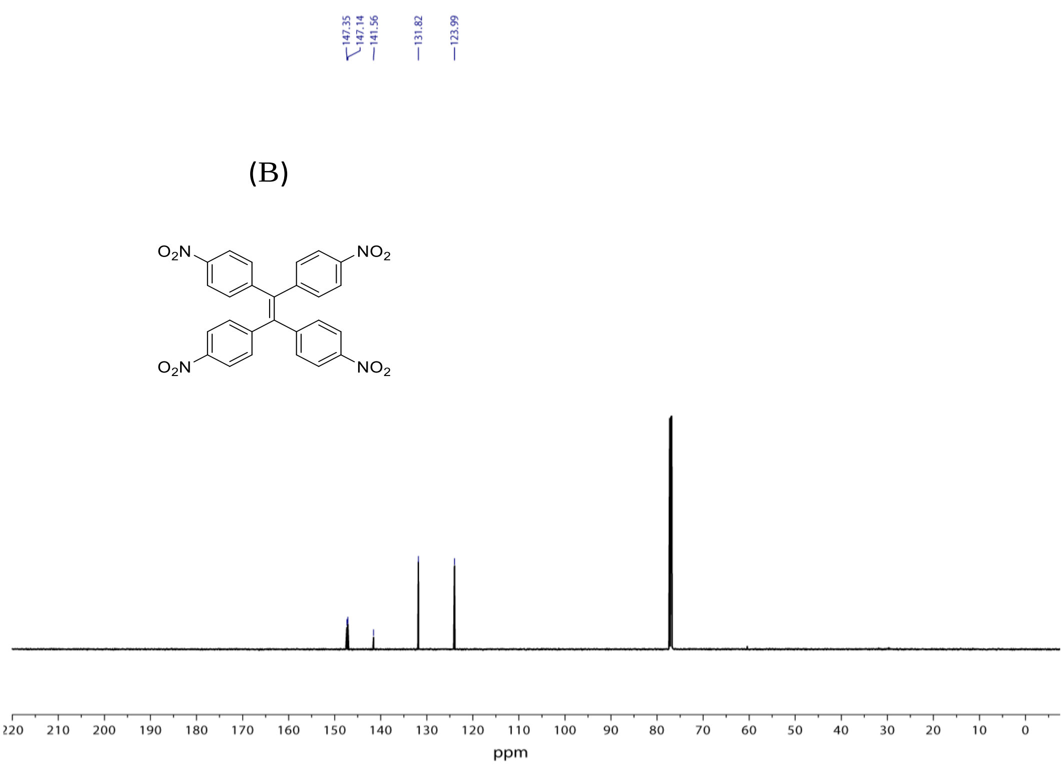

Fig. S36 ^{1}H NMR (A) and ^{13}C NMR (B) spectra of compound **TPE-NO$_2$**.

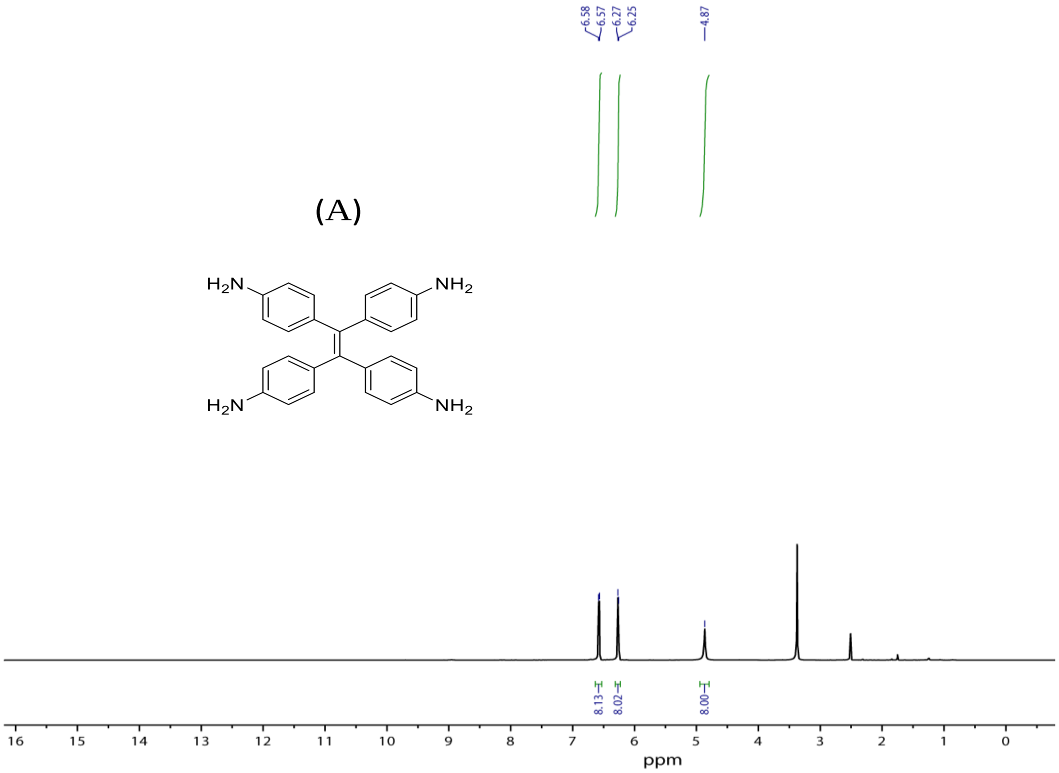

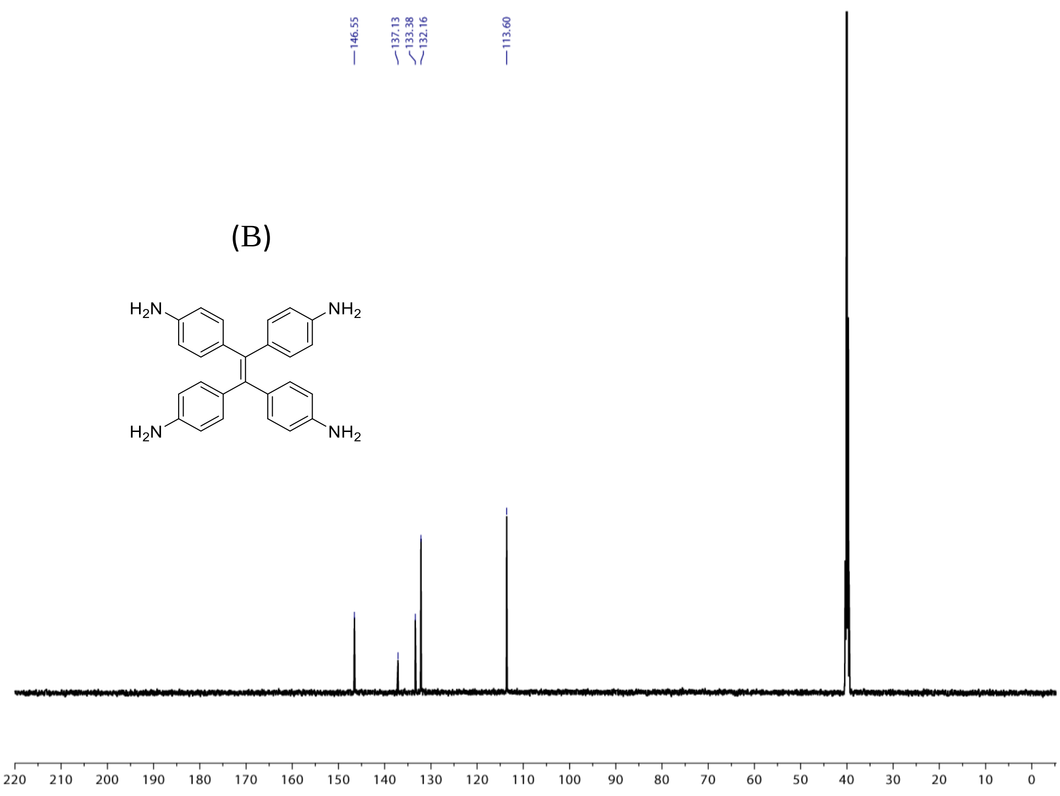

Fig. S37 ^{1}H NMR (A) and ^{13}C NMR (B) spectra of compound **TPE-NH$_2$**.

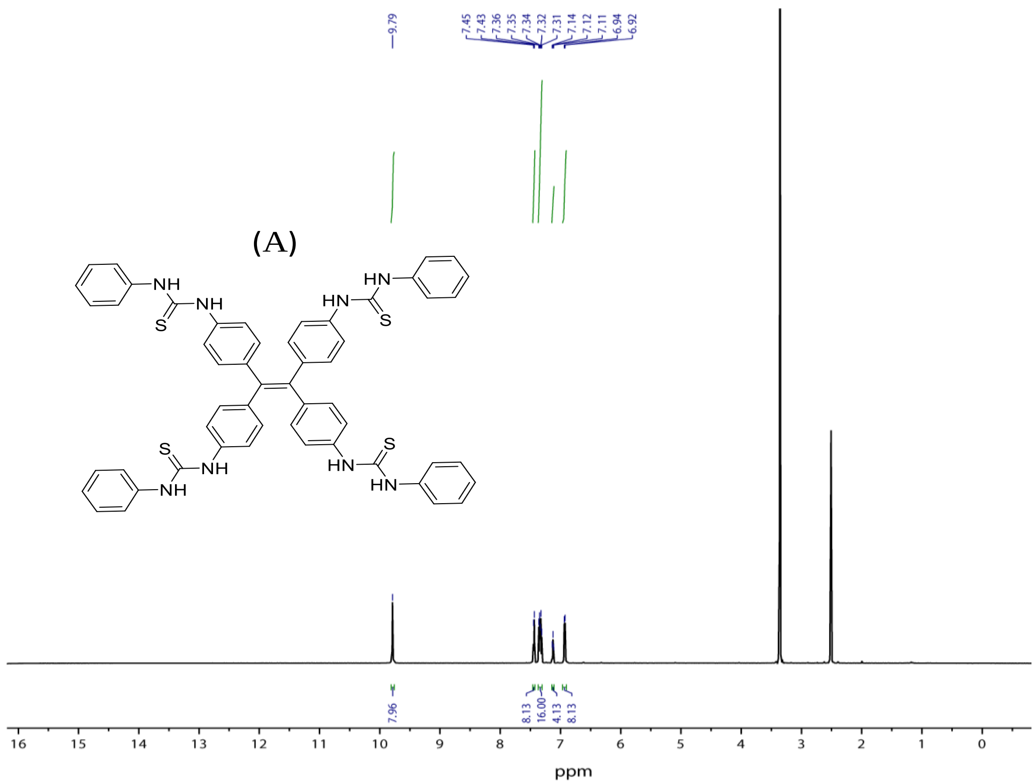

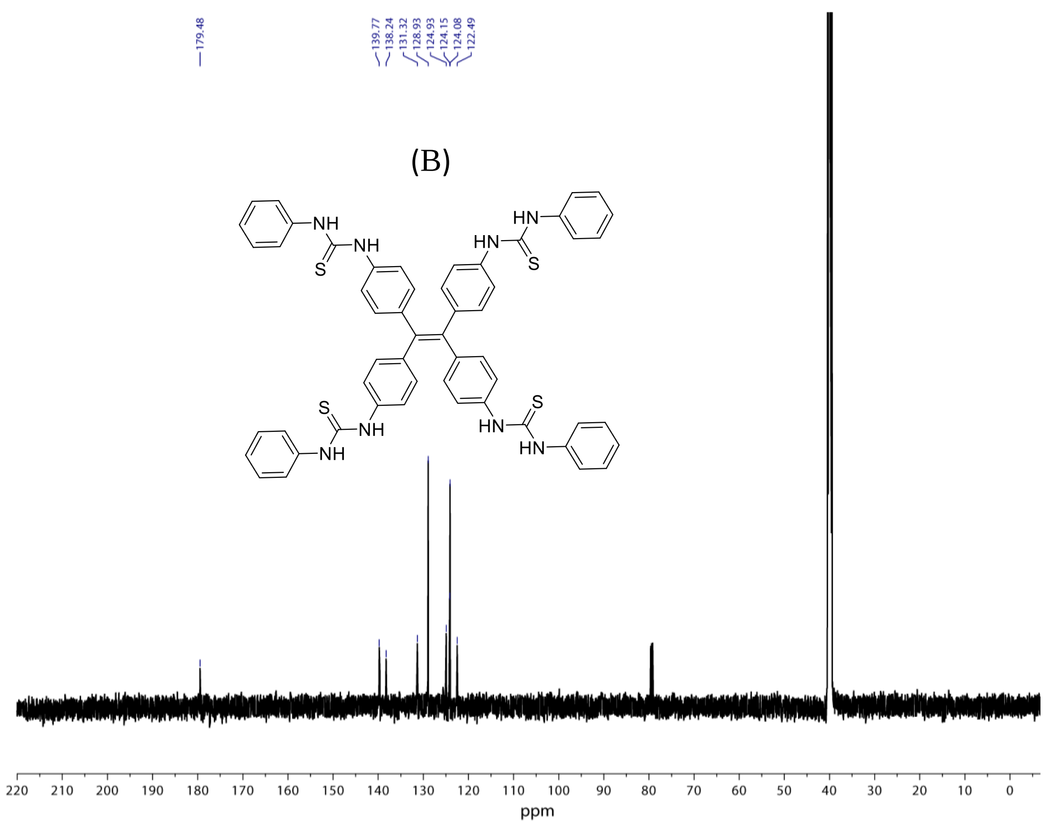

Fig. S38 ^{1}H NMR (A) and ^{13}C NMR (B) spectra of compound **1a**.

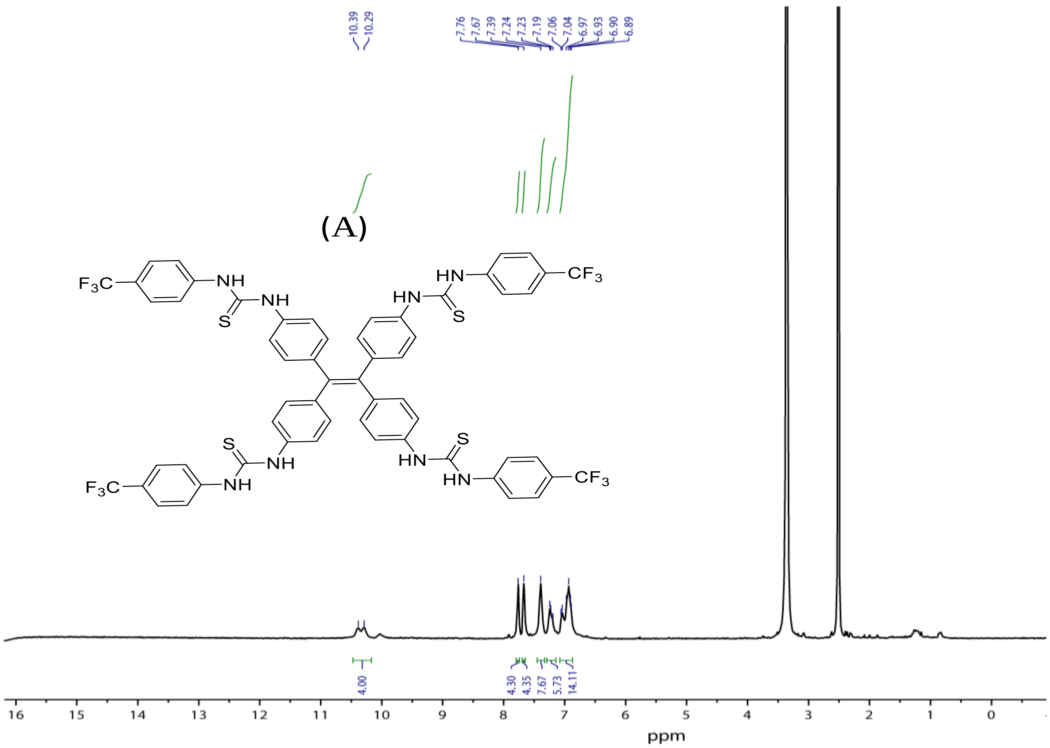

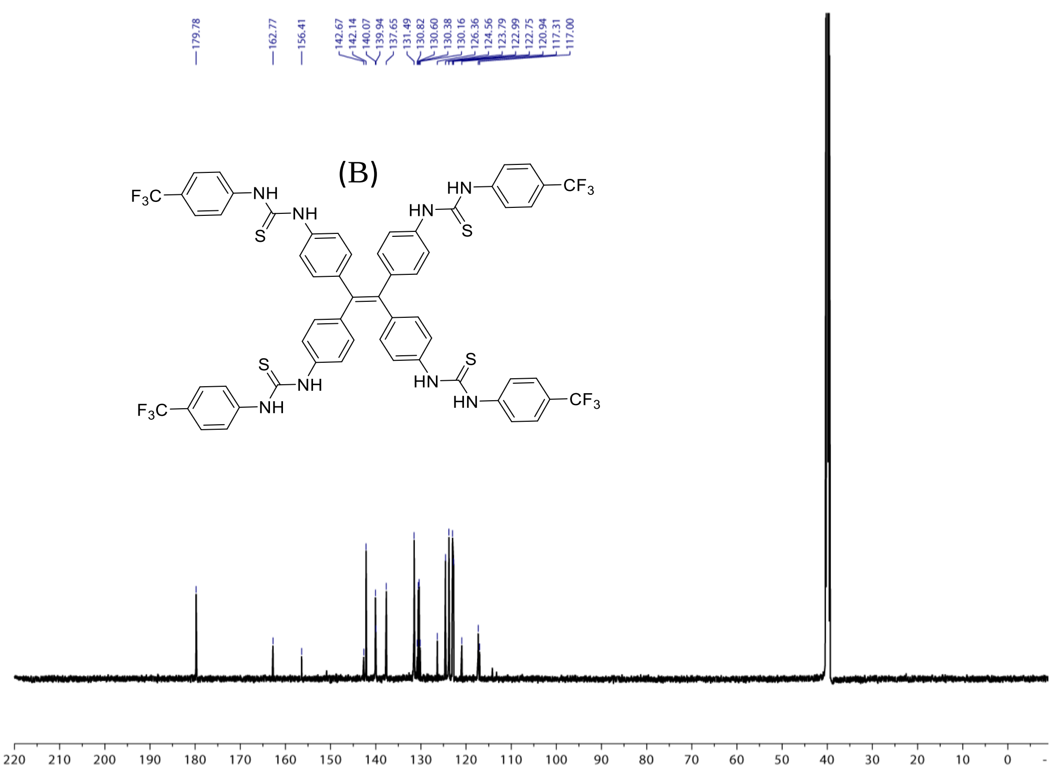

Fig. S39 ^{1}H NMR (A) and ^{13}C NMR (B) spectra of compound **1b**.

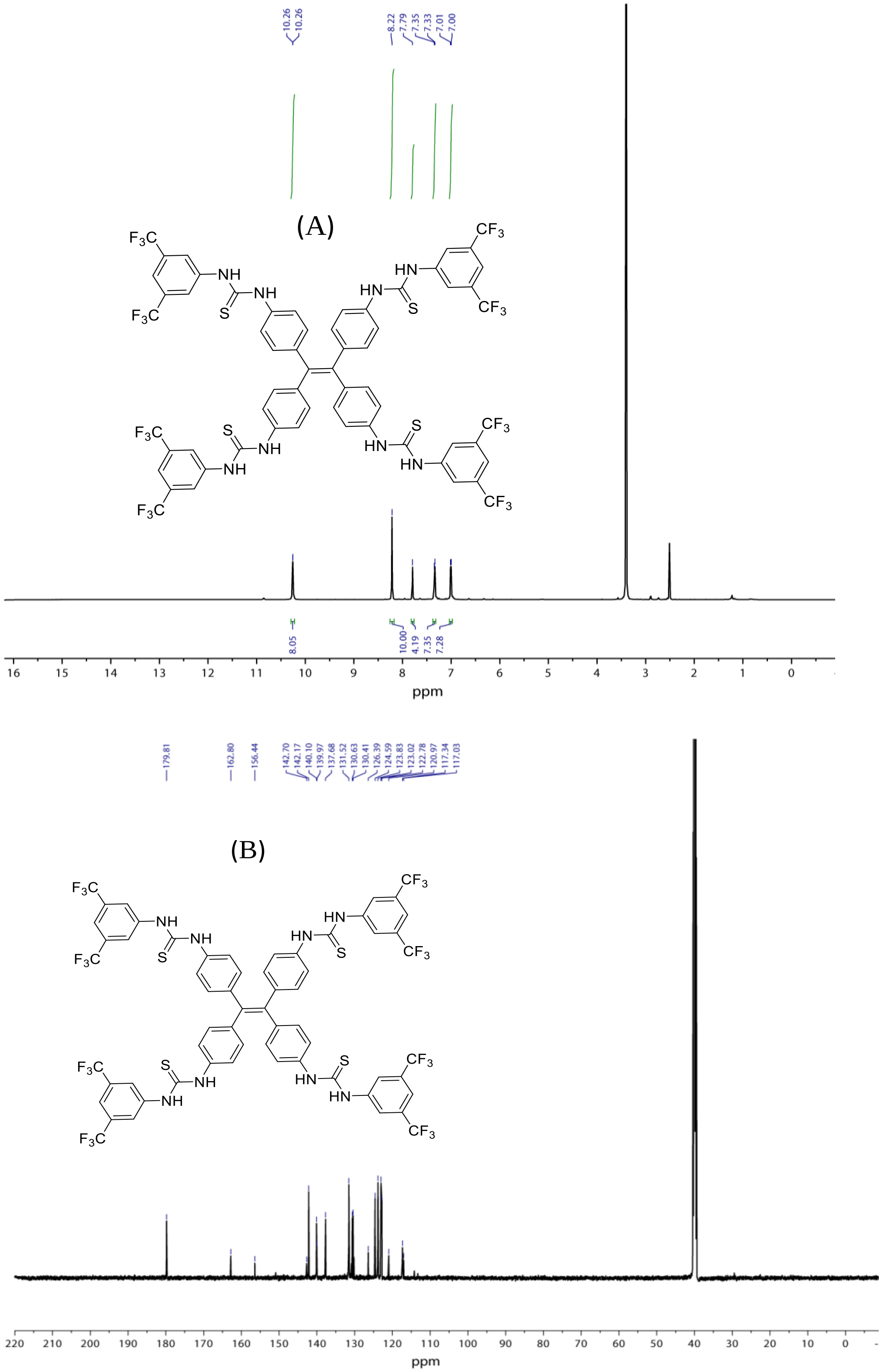

Fig. S40 ^{1}H NMR (A) and ^{13}C NMR (B) spectra of compound **1c**.

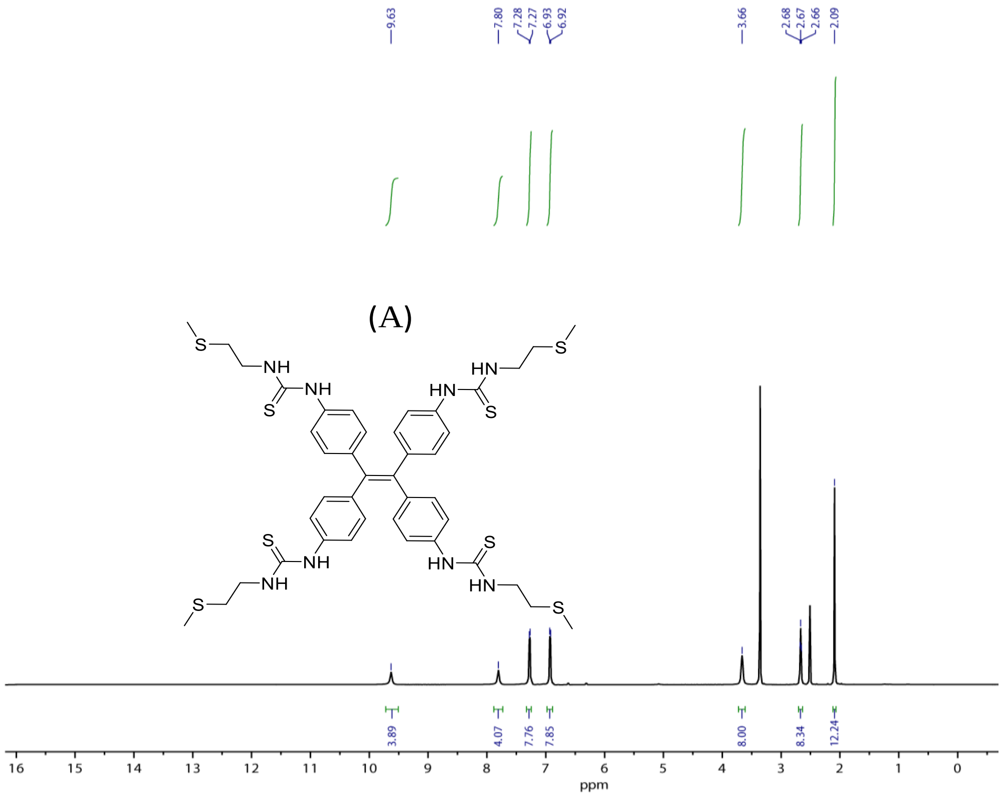

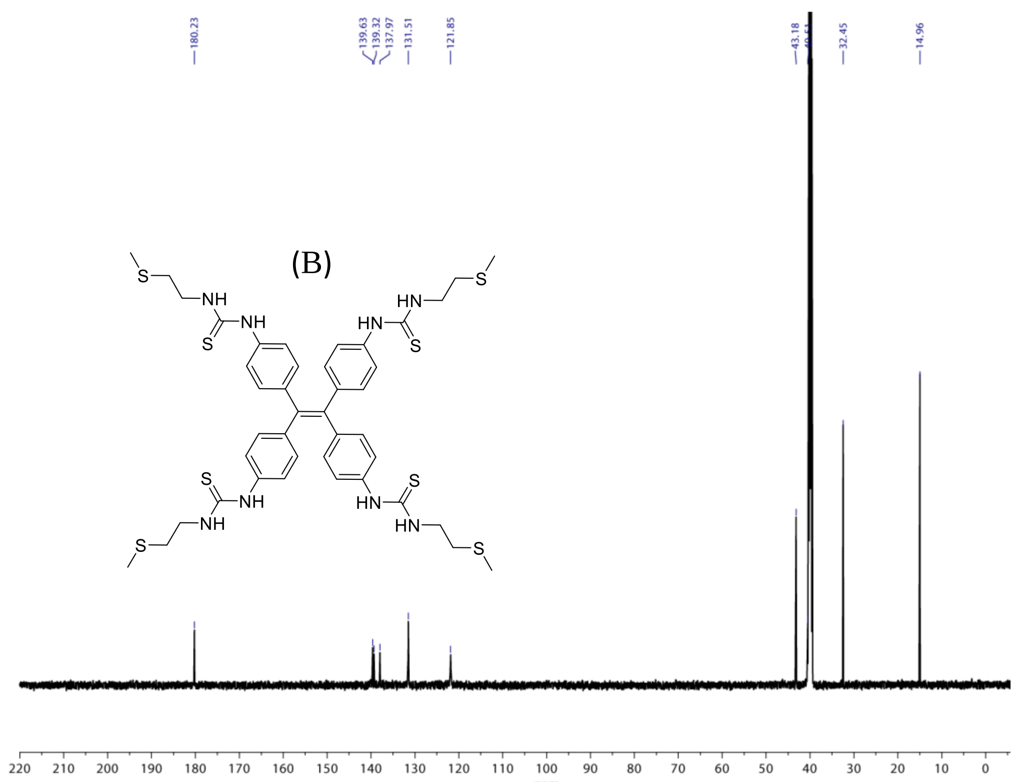

Fig. S41 ^{1}H NMR (A) and ^{13}C NMR (B) spectra of compound **1d**.

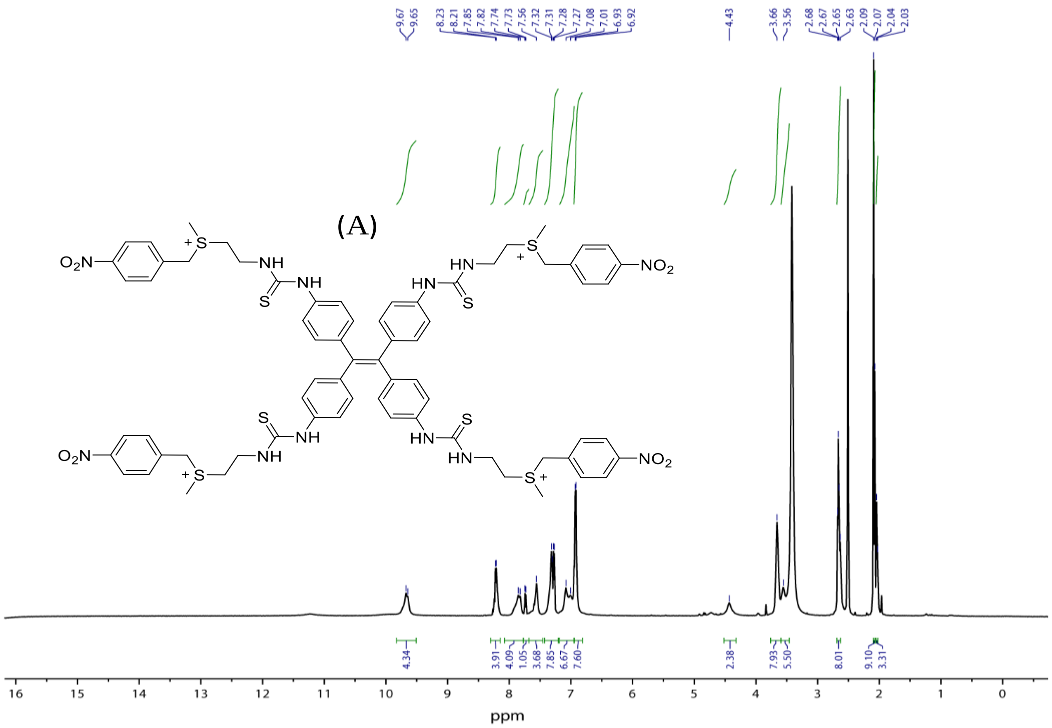

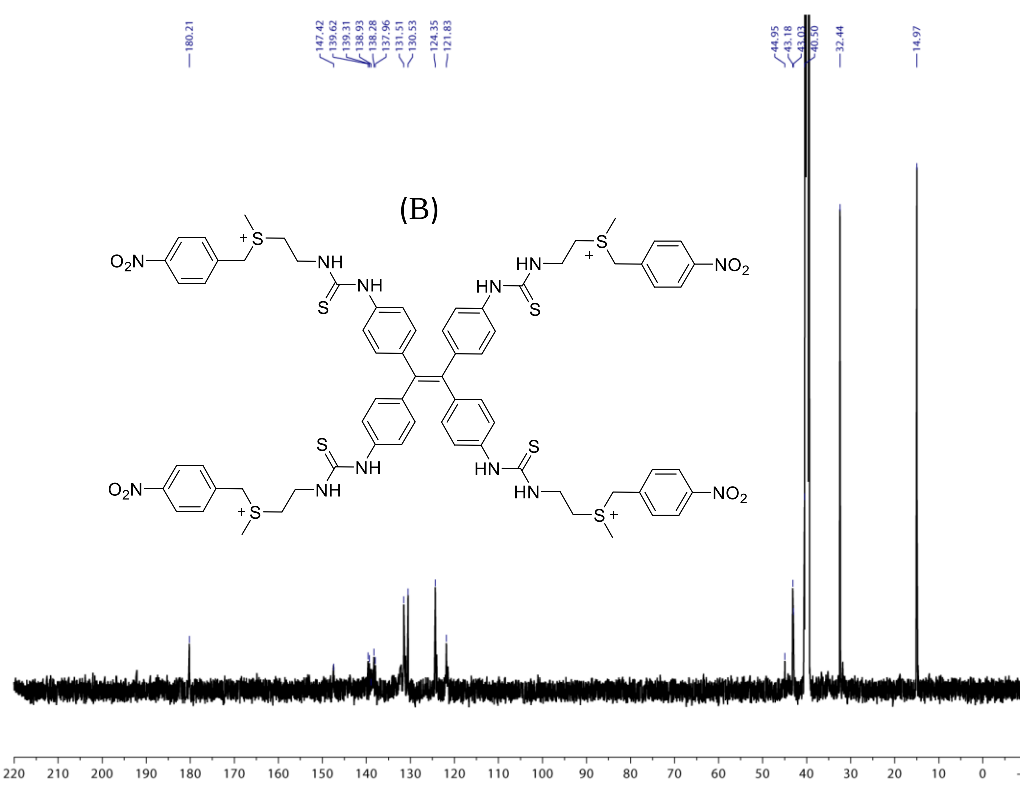

Fig. S42 ^{1}H NMR (A) and ^{13}C NMR (B) spectra of compound **2**.